https://doi.org/10.5194/egusphere-2026-1673
Preprint. Discussion started: 8 April 2026

Land carbon response to positive, zero, and negative CO_2 emissions across Earth system models

Abigail L. S. Swann[1,2], Charles D. Koven[3], Cristian Proistosecu[4,5], Rosie A. Fisher[6], Benjamin M. Sanderson[6], Victor Brovkin[7,8], Tomohiro Hajima[9], Chris D. Jones[10,11], Nancy Y. Kiang[12,13], David M. Lawrence[14], Spencer Liddicoat[11], Hannah Liddy[13], Anastasia Romanou[12,15], Roland Séférian[16], Lori T. Sentman[17], Norman J. Steinert[6], Jerry Tjiputra[18], and Tilo Ziehn[19]

[1]Department of Atmospheric and Climate Science, University of Washington, Seattle, WA, USA
[2]Department of Biology, University of Washington, Seattle, WA, USA
[3]Lawrence Berkeley National Laboratory, Berkeley, USA
[4]Department of Climate, Meteorology, and Atmospheric Science, University of Illinois Urbana Champaign, Urbana, IL, USA
[5]Department of Earth Sciences and Environmental Change, University of Illinois Urbana Champaign, Urbana, IL, USA
[6]CICERO International Center for Climate Research, Oslo, Norway
[7]Max Planck Institute for Meteorology, Hamburg, Germany
[8]University of Hamburg, Hamburg, Germany
[9]Research Institute for Global Change, Japan Agency for Marine-Earth Science and Technology, Yokohama, Japan
[10]School of Geographical Sciences, University of Bristol, UK
[11]Met Office Hadley Centre, Exeter, UK
[12]NASA Goddard Institute for Space Studies, New York, NY, USA
[13]Center for Climate Systems Research, Columbia University, New York, NY, USA
[14]NSF National Center for Atmospheric Research, Boulder, CO, USA
[15]Dept. Applied Phys. Applied Math., Columbia U., New York, NY, USA
[16]Météo-France, CNRS, Univ. Toulouse, CNRM, Toulouse, France
[17]NOAA/Geophysical Fluid Dynamics Laboratory, Princeton, NJ, USA
[18]NORCE Research AS, Bjerknes Centre for Climate Research, Bergen, Norway
[19]CSIRO Environment, Aspendale, Australia

Correspondence: Abigail L.S. Swann (aswann@uw.edu)

Abstract. Land carbon sinks are responsible for removing about a quarter of anthropogenic CO_2 emissions, and make up approximately half of total global carbon sinks. Uncertainty in the response of land carbon sinks to climate and changing atmospheric CO_2 are large, and dominate the uncertainty in total carbon sinks under future climate. Understanding the carbon cycle response to net-zero and net-negative emissions has important implications for projecting future climate. Experiments in the 'flat10' model intercomparison were designed for directly estimating key climate metrics that underlie carbon budgeting frameworks. Here we characterize the response of land carbon pools and fluxes from ten emissions-driven Earth system models (ESMs) under positive, net-zero, and net-negative CO_2 emissions. Although there are many differences in simulated land carbon pools and fluxes across models, we find some consistent behavior across ESMs. 1) During the positive emissions phase, carbon is gained on land primarily in vegetation pools. 2) Following net-negative emissions to the point of cumulative zero emissions, carbon is lost from land in tropical latitudes, primarily from vegetation pools, but in mid- and high-latitudes most models show net land carbon gain, primarily in soil pools. 3) Following an extended period of net-zero emissions, a majority

https://doi.org/10.5194/egusphere-2026-1673
Preprint. Discussion started: 8 April 2026

of models again show carbon gain in mid- and high-latitudes and vegetation carbon loss in the tropics. Under net-negative emissions the timing of vegetation carbon response relative to peak emissions is relatively consistent across ESMs, but timing of soil carbon response varies widely, implying larger intermodel disagreement associated with responses of soil carbon which tends to have longer timescales relative to vegetation carbon. Our findings highlight that tropical carbon is most likely to be both gained and subsequently lost under positive, zero, declining, and negative emissions, with possible implications for carbon dioxide removal efforts.

1 Introduction

Terrestrial systems remove carbon from the atmosphere through photosynthesis, and release carbon through respiration, fire, and other pathways. The balance of these processes results in a net flux that represents either a source to or sink of carbon from the land to the atmosphere. Anthropogenic emissions of CO_2 into the atmosphere since the industrial revolution, including emissions from fossil fuel burning, cement production, and anthropogenic land cover and land use change, have been partially balanced by land and ocean carbon sinks, where here we define land sink as the net removal of CO_2 from the atmosphere by natural vegetation and agriculture. Over the industrial period, 755 $\pm$65 PgC of anthropogenic CO_2 has been emitted to the atmosphere. Of this, terrestrial carbon sinks are estimated to have removed about 24%, or 175 $\pm$50 PgC, with 27% going into ocean sinks and 39% remaining in the atmosphere and leading to increased atmospheric CO_2 concentrations. Over the period 1959-2024 a 1 PgC/yr imbalance remains in the assessed global carbon budget (Friedlingstein et al., 2025).

The net terrestrial carbon sink reflects the balance of many biological mediated processes that depend on climatic conditions and atmospheric CO_2 concentrations. Leaf level photosynthesis has the potential to increase as the partial pressure of CO_2 in the atmosphere increases, at least at concentrations experienced up to this date (Bonan, 2015; Ficklin and Novick, 2017; Grossiord et al., 2020; Zhang et al., 2019). However, photosynthesis is also co-limited by irradiance, temperature, moisture stress, and nutrient availability; therefore, enhancement by increasing atmospheric CO_2 is limited. It is theorized that such limitations will become more widespread as temperatures continue to increase and rainfall patterns shift (e.g. Xu et al., 2019; Zhang et al., 2025), even considering possible acclimation of photosynthetic processes to temperature change (Yamori et al., 2014; Kumarathunge et al., 2019). Respiration releases carbon, both from autotrophic and heterotrophic sources. Generally respiration rates increase with warming, but acclimation may also moderate the response of respiration to temperature (Reich et al., 2016; Atkin and Tjoelker, 2003), and the specific rates also depend on microbial community composition (Wieder et al., 2013). The fact that land has served as a carbon sink during the historical period suggests that, to date, enhanced photosynthesis has outpaced increases in respiration.

Projections of future terrestrial carbon sinks by Earth system models (ESMs) were first systematically compared in modeling experiments that were part of the Coupled Climate Carbon Cycle Model Intercomparison Project (C4MIP, Friedlingstein et al., 2006), where the spread across models was large, and substantially larger than the spread across estimates of ocean carbon sinks. Many elements of the terrestrial carbon cycle are heterogenously represented, poorly understood and/or subject to significant parametric uncertainty, leading to these large divergences in model projections. The C4MIP effort has been repeated in

https://doi.org/10.5194/egusphere-2026-1673
Preprint. Discussion started: 8 April 2026

the intervening years with newer generations of ESMs, but spread in estimated land carbon sinks across models has remained stubbornly large (Friedlingstein et al., 2014; Arora et al., 2020; Liddicoat et al., 2021). Not only is the spread in land carbon sink across models large, but the possible spread within a single model is also large. For example, projections made with the CMIP3-era HadCM3 ESM spanned ∼450 ppm in atmospheric CO_2 in 2100 in response to modified assumptions within the land model (Booth et al., 2012). This lack of consensus across projections of the future land carbon sink likely stems from the fact that many biological processes contribute to the land carbon sink outcome, each of them remains individually uncertain, and the number of model implementations is very small compared the dimensionality of that uncertainty, though recent developments in model emulation and parameter constraints against data show some promise in restricting the range of projections (McNeall et al., 2024).

Anthropogenic CO_2 that accumulates in the atmosphere causes radiative forcing, with resulting changes to climate including increasing surface temperature. Many physical climate and carbon cycle processes contribute to the uncertainty in climate response to radiative forcing (Jones and Friedlingstein, 2020; Jeevanjee et al., 2025). The Earth system during the historical period shows an emergent near linear response of globally averaged surface temperature to the cumulative emissions of CO_2 (Allen et al., 2009; Matthews et al., 2009; Meinshausen et al., 2009). ESMs also show this linear behavior, called the "transient climate response to cumulative CO_2 emissions" (TCRE) (Allen et al., 2009; Matthews et al., 2009; Zickfeld et al., 2009), across a range of different CO_2 emissions pathways ranging from high to low emissions, and from complex to idealized scenarios (Canadell et al., 2021). The proportionality of warming to cumulative emissions suggests that temperatures will become stable when cumulative emissions stop growing, as happens when annual emissions go to zero. How the Earth system will respond to a cessation in emissions is quantified using the term "zero emissions commitment" (ZEC), which is the change in global mean temperature after annual emissions reach zero (Matthews and Caldeira, 2008; Solomon et al., 2009). ESM experiments suggest that after zero emissions are reached, cooling caused by the removal of atmospheric CO_2 through continued land and ocean carbon uptake is largely balanced by warming caused by reductions in ocean heat uptake, with the net result being relatively stable global mean temperatures and a ZEC of 0 ± 0.3 (Jones et al., 2019; MacDougall et al., 2020).

Existing ESM experimental protocols have not included estimates of ZEC that are consistent across ESMs and relevant in emission-driven frameworks. ZECMIP (Jones et al., 2019) experiments were used to estimate ZEC previously, using diagnosed emissions that are unique to each model. This model-specific emissions rate results in inconsistencies between the timescales for thermal responses and the timescales for carbon cycle responses across models. To resolve this, a new experimental design for estimating TCRE and ZEC has recently been proposed and adopted for use in the coupled model intercomparsion project version 7, called 'flat10MIP' (Sanderson et al., 2025). The flat10MIP set of experiments uses emissions-driven ESMs to simulate the coupled carbon cycle response to specified idealized emissions, including constant emissions near present-day rates, as well as an abrupt transition to zero emissions and a ramp-down of emissions to zero and then net-negative emissions. Prior experiments were based on specified concentrations of CO2, diagnosing distinct emissions timeseries for each model. The flat10MIP experiments use specified emissions which makes the assessment of TCRE and ZEC direct and straightforward, as both metrics are specified relative to cumulative or annual emissions. Nine ESMs participated in the initial model

https://doi.org/10.5194/egusphere-2026-1673
Preprint. Discussion started: 8 April 2026

intercomparison using this experimental design (see the methods section for details of the flat10 experiments, Sanderson et al., 2025).

Understanding the carbon cycle response to net-zero and net-negative emissions, and particularly the highly uncertain land carbon cycle response, has important implications for projecting future climate. Intriguing behavior of the carbon cycle has been observed in low emissions scenarios (e.g. SSP1-1.9, Koven et al., 2022), yet most model intercomparisons using emissions-driven ESMs have focused on regimes of increasing emissions, with only a limited number of simulations completed for lower or negative emissions scenarios (Asaadi et al., 2024). The flat10MIP experiments offer a new opportunity to systematically compare the response of terrestrial carbon cycling to zero and net-negative emissions across a larger array of ESMs. TIPMIP (Jones et al., 2025) is another newly proposed intercomparison project with a goal of assessing models at equal rates of warming. The TIPMIP experimental design uses model-specific emissions rates to achieve equal warming rates at a specified time point. The response of carbon cycling under equal rates of emissions (as in flat10MIP) may differ from the response under equal amounts of warming (as in TIPMIP) and any such differences may provide insight into the relative roles of carbon and heat uptake in setting ZEC.

Here we report responses of the flat10MIP experiments, focusing on characterizing the response of land carbon pools and fluxes to specified emissions in ten ESMs. All ten ESMs performed the three flat10MIP scenarios, including positive, net-zero, and net-negative emissions (wherein all emitted carbon is removed to the point where cumulative emissions reach zero). In the methods we provide brief descriptions of each model and describe relevant components of their land carbon cycles. In results and discussion we describe the initial carbon stocks in each model, their response to change during the positive emissions phase, net-zero phase, and during net-negative and at cumulative zero emissions. Finally, we present the timing of carbon pool responses relative to emissions under declining and negative emissions. We finish with conclusions and implications.

2 Data and Methods

2.1 flat10MIP experiments

The flat10MIP experimental design, described in Sanderson et al. (2025), consists of idealized experiments designed for efficiently assessing both TCRE and ZEC. Here we evaluate three flat10MIP experiments (Fig. 1). The first is the "flat10" experiment (esm-flat10), wherein carbon is emitted to the atmosphere at 10 PgC/yr. This experiment was continued for between 150 and 300 years depending on the ESM. At 100 years, the point where cumulative emissions is at 1000 PgC, two experiments were branched. In the "flat10-zec" experiment (esm-flat10-zec), emissions are set to zero following the "flat10" increase, and the simulation is continued for 200 years. In the "flat10-cdr" experiment (esm-flat10-cdr), emissions decline by 0.2 PgC/yr, reaching zero emissions at 50 years. Emissions then become negative and continue declining by 0.2 PgC/yr until reaching -10 PgC/yr at year 100. The simulation is continued for an additional 100 years at -10 PgC/yr emissions. Here we consider the esm-flat10-zec and esm-flat10-cdr experiments as a continuous time series with the initial 100 years from the esm-flat10 experiment, and the following 200 years from each of the protocols described above. Thus the point of zero

https://doi.org/10.5194/egusphere-2026-1673
Preprint. Discussion started: 8 April 2026

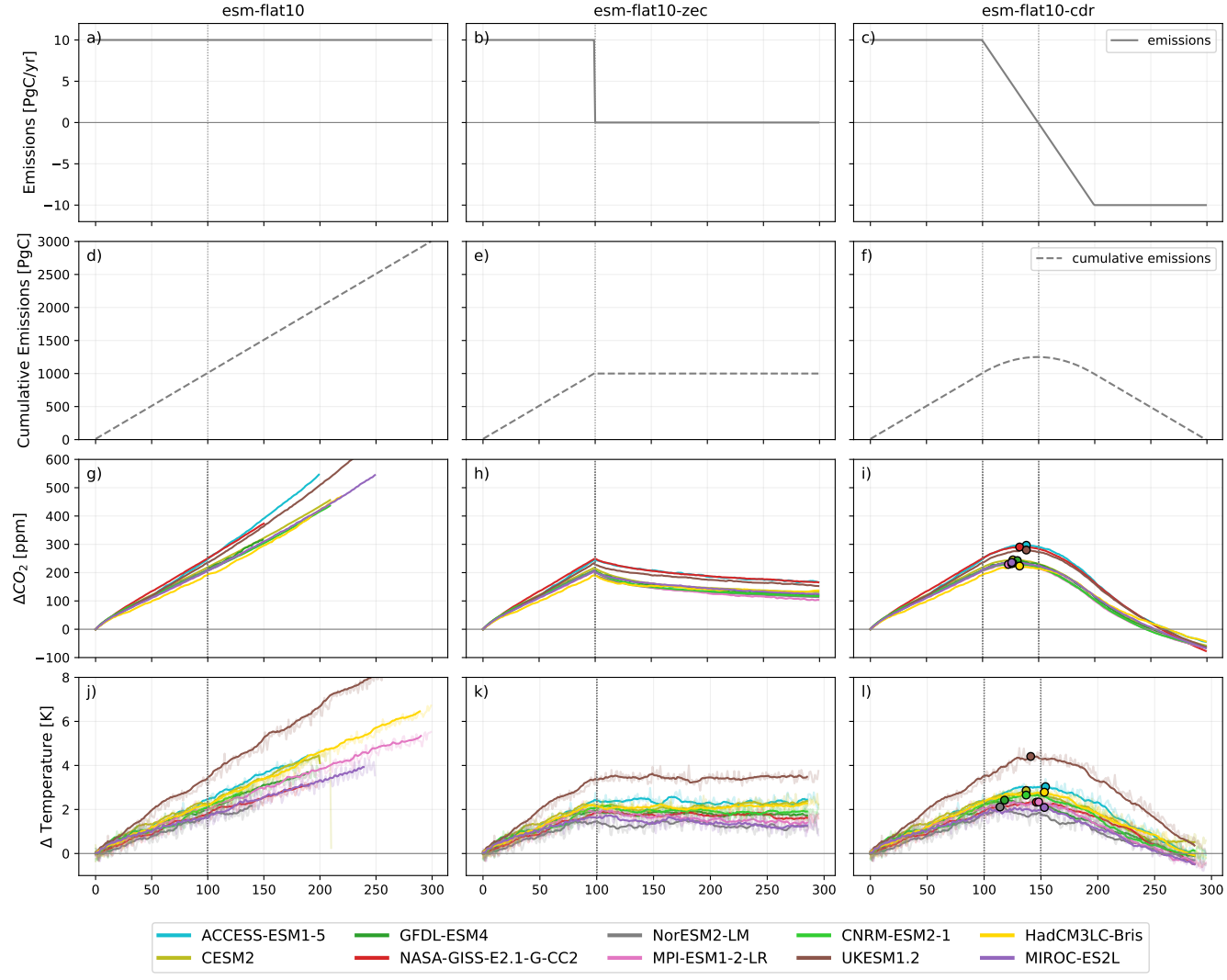

Figure 1. Global mean timeseries emissions, cumulative emissions, temperature, and CO_2. Time series of annual emissions (top row), cumulative emissions (second row), change in global mean atmospheric CO_2 (third row), and temperature. Columns show each of the three experiments: esm-flat10 (left), esm-flat10-zec (middle), and esm-flat10-cdr (right). Each line in the second and third rows represents one ESM participating in flat10MIP. Colored circles indicate the year of peak CO_2 or temperature during the esm-flat10-cdr experiment.

emissions is reached at year 100 in esm-flat10-zec and at year 150 in esm-flat10-cdr. At year 300 in esm-flat10-cdr scenario, cumulative emissions over the whole time period have reached zero.

We analyze both the full time series as well as distinct time windows within these simulations. We report initial carbon stocks (Initial C) as the average over the first 10 years of the esm-flat10 experiment. We report changes in carbon stocks at the end of the emissions phase (Δ Emissions Phase) as the difference between the average around 1000 PgC of cumulative

https://doi.org/10.5194/egusphere-2026-1673
Preprint. Discussion started: 8 April 2026

emissions in the esm-flat10 experiment (20 years centered on year 100) and the Initial C, while noting that this is the average over a transient period with increasing cumulative emissions for the first 10 years. We report the change in carbon following zero emissions (Δ Net-zero) as the average of the end of the esm-flat10-zec experiment (last 10 years) minus carbon stocks at the end of the emissions phase (20 years centered on year 100). We report the change in carbon at cumulative zero emissions (Δ Cumulative-zero) as the average of the end of the esm-flat10-cdr experiment (last 10 years) minus the initial carbon pools.

2.2 Terrestrial carbon cycle representation in each ESM

2.2.1 ACCESS-ESM1-5

ACCESS-ESM1-5 (Ziehn et al., 2020) uses the CABLE land surface model (Kowalczyk et al., 2013) with biogeochemistry implemented through the CASA-CNP module, which includes the carbon cycle with added nitrogen and phosphorus cycles (Wang et al., 2010). The CABLE configuration in ACCESS-ESM1-5 uses 10 vegetation land cover types and a prognostic leaf area index based on the size of the leaf carbon pool and the specific leaf area. The flow of carbon and nutrients is simulated between three plant biomass pools (leaf, wood, root), three litter pools (metabolic, structural, coarse woody debris) and three organic soil pools (microbial, slow, passive) plus additional nitrogen (inorganic) and phosphorus (labile, sorbed, strongly sorbed) soil pools. All simulations have been run with nitrogen and phosphorus limitation enabled.

2.2.2 CESM2

The terrestrial carbon cycle in CESM2 (Danabasoglu et al., 2020) used v5 of the Community Land Model (CLM5, Lawrence et al., 2019), a big-leaf representation of coupled carbon and nitrogen cycling, which includes representations of permafrost, crops, methane cycling, urban, lake, glaciated and bare ground land cover types. CLM5 contains a hydrodynamic representations of plant drought stress and soil moisture uptake (Kennedy et al., 2019), as well as representations of shifts in plant nutrient acquisition between active uptake and fixation (Fisher et al., 2019). Temperature acclimation of both photosynthesis and respiration is represented (Lombardozzi et al., 2015). The responses of carbon cycling to inter-annual variability in moisture availability are lower, and the response to CO_2 fertilization greater than in previous version of the CLM (Wieder et al., 2019).

2.2.3 GFDL-ESM4

The NOAA Geophysical Fluid Dynamics Laboratory (GFDL) ESM4 model (Dunne et al., 2020) includes the GFDL Land Model version 4.1 (LM4.1, Shevliakova et al., 2024) dynamic land vegetation component. Land hydrology and ecosystem dynamics are represented on the same 1^o grid as the GFDL Atmospheric Model version 4.1 (AM4.1, Horowitz et al., 2020) atmospheric component, which includes interactive aerosols and chemistry. The ocean is represented by GFDL's open source Modular Ocean Model version 6 (MOM6, Adcroft et al., 2019) physical ocean component, the Carbon, Ocean Biogeochemistry and Lower Trophics version 2 (COBALTv2, Stock et al., 2020) ocean biogeochemical component, and Sea Ice Simulator version 2 (SIS2, Adcroft et al., 2019) sea ice component. In GFDL-ESM4, carbon is fully coupled and interactive among these

https://doi.org/10.5194/egusphere-2026-1673
Preprint. Discussion started: 8 April 2026

components. The Coupled Climate-Carbon Cycle Model Intercomparison Project (C4MIP) guideline for quasi-equilibrium (0.1 PgC/yr Jones et al., 2016) was established during the first two centuries of preindustrial spin-up integration, prior to participation in the Coupled Model Intercomparison Project phase 6 (CMIP6, Eyring et al., 2016). The flat10MIP simulations were initialized from year 101 of the CMIP6 GFDL-ESM4 emissions-driven preindustrial control simulation.

LM4.1 represents sub-grid scale heterogeneity of the land surface via a mosaic approach that divides each land grid cell into multiple tiles, each representing unique physical and biological properties. Within each tile, LM4.1 represents multiple vegetation cohorts per layer, of different ages and vegetation types, with cohort-specific energy balance and intercepted water/snow. Radiation treatment includes multistory canopy dynamics, with transpiration and stomatal conductance based on Wolfe et al. 2016. Prognostic vegetation distribution dynamics are represented by a fully consistent explicit treatment of ecosystem demography, multi-layer vegetation canopy, and land surface processes, and include age-height structured vegetation competition for light – the Perfect Plasticity Approximation (PPA, Purves and Pacala, 2008; Weng et al., 2015). LM4.1 includes 6 plant functional types (PFTs) in representing C3 grass, C4 grass, tropical trees, temperate deciduous trees, and cold evergreen trees. 6 live carbon pools in LM4.1 represent leaves, fine roots, heartwood, sapwood, seeds, and non-structural carbon (i.e., sugars). Carbon gain is allocated daily to leaves, fine roots, sapwood, seeds, and non-structural carbon pools according to the tree-grass allometric relationship (Martínez Cano et al., 2020; Weng et al., 2015).

Soil carbon dynamics and biogeochemistry are represented by the Carbon, Organisms, Rhizosphere, and Protection in the Soil Environment (CORPSE, Sulman et al., 2014, 2019) model. Litter is divided into leaf and coarse-wood categories, and into fast- and slow-timescale partitions. Each of the 20 vertical soil levels represents separate fast and slow soil carbon pools, along with two carbon storage pools associated with soil microbes and microbial products. Land use in LM4.1 occurs through annual wood harvesting, divided into secondary tiles by age, crop planting and harvesting at specified times of the year, and daily grazing on pastures (5% per day), as well as on rangelands – vegetation taller than 3 m that is not grazed (Hurtt et al., 2020). LM4.1 includes the FINAL v2 fire model (Rabin et al., 2015, 2018; Ward et al., 2018)(Rabin et al., 2015, 2018; Ward et al., 2018) representing daily fire, including both multi-day and crown fires. Dust emissions are based on surface wind, snow fraction, soil ice, surface LAI and SAI bareness, and land use (Evans et al., 2016, 2019) as simulated for each LM4.1 tile, and passed to the atmosphere. The LM4.1 component in GFDL-ESM4 does not include an interactive nitrogen cycle and does not formally represent long-term permafrost cycling. Instead, a 500-year maximum soil lifetime is included to prevent accumulation of recalcitrant material under cold, dry conditions and to achieve land carbon equilibration.

2.2.4 NASA-GISS-E2.1-G-CC2

The NASA Goddard Institute for Space Studies ESM ModelE, version NASA-GISS-E2.1-G-CC2 (Romanou et al., 2026) has a coupled carbon cycle (Ito et al., 2020b) that uses the Ent Terrestrial Biosphere Model (Ent TBM, Kim et al., 2015) for land carbon dynamics and an updated version of the NASA Ocean Biogeochemistry Model (NOBM) (Romanou et al., 2013, 2014), coupled through atmospheric CO_2 tracers (Romanou et al., 2013, 2014). The Ent TBM simulates 12 plant functional tyeps (PFTs), including one crop type. Canopy radiative transfer is a layered, two-stream scheme of (Spitters et al., 1986), with canopy albedo otherwise prescribed from a translation of (Matthews, 1983) to Ent PFTs. Leaf biophysics has coupled photo-

https://doi.org/10.5194/egusphere-2026-1673
Preprint. Discussion started: 8 April 2026

synthesis (Farquhar and Von Caemmerer, 1982) and stomatal conductance (Ball et al., 1987) with a leaf boundary layer (Collatz et al., 1991). C4 photosynthesis is based on (Collatz et al., 1998). Drought stress is simulated by limiting stomatal conductance based on a linear relation to PFT-dependent critical relative soil saturation values following (Rodriguez-Iturbe et al., 2001). Soil biogeochemistry is the CASA' model (Randerson et al., 2009; Doney et al., 2006), with 9 soil carbon pools and updated soil moisture sensitivity (Kim et al., 2015). The 9 soil carbon pools are simulated in one soil layer averaging the upper 30 cm of soil microclimate. For land cover change, the model prescribes historical crop cover as a single crop PFT. Photosynthetic uptake of carbon is stored in a labile non-structural carbohydrate pool, which is withdrawn for autotrophic respiration, seasonal leaf growth, allocation to a reproductive pool, and stem growth, as well as replenished through retranslocation from senescing foliage. Crop cover changes once per year, proportionally rescaling the natural vegetation types by grid cell. To conserve carbon with annual cover change, the net change in land carbon stocks is distributed as fluxes to the atmosphere uniformly over the following year to avoid an annual pulse in atmospheric CO_2. The Ent TBM does not currently include nitrogen dynamics, land use state transition, wood harvest, deforestation, fire, or community dynamics or mortality and establishment.

For this study, the Ent TBM was run in a configuration with "biophysics-only" dynamics, in which vegetation boundary conditions (cover fraction, canopy heights, leaf area index) were prescribed from a satellite-derived observational data set, as described in (Ito et al., 2020b). Crop cover was prescribed from the Land Use Harmonization version 2 (LUH2) data set (Hurtt et al., 2020), using the updated years from the Global Carbon Budget project (Friedlingstein et al., 2024), combining all LUH2 crop cover types into one Ent C3 crop type. In the biophysics mode with fixed vegetation structure, the prognostic land carbon pools are the plant labile carbon and soil carbon pools. The labile carbon pool balance is subject to the same fluxes of respiration and allocation/retranslocation, but not reproduction, and the carbon that would be allocated to stem growth is instead dropped as litterfall to the soil. To prevent carbon deficits, at low labile carbon balances, autotrophic respiration is reduced or turned off rather than causing mortality, until the labile carbon pool replenishes. Therefore, enhanced carbon uptake due to the CO_2 fertilization effect is expressed in the biophysics-only mode as increased litterfall. The enhanced litterfall is not inconsistent with the increased turnover that can happen with CO_2 fertilization without increases in biomass in mature ecosystems, and with increased soil carbon storage, as observed in the tropics by (Bar-On et al., 2025). The simulation was first spun up to equilibrate the soil carbon pools before conducting transient simulations through the flat10 experimental protocol.

2.2.5 NorESM2-LM

The land carbon cycle in NorESM2-LM (Seland et al., 2020) is based on the Community Land Model 5 (CLM5, Lawrence et al., 2019). It simulates the carbon and nitrogen cycles, including natural vegetation, litter, and soil carbon pools. In addition to temperature and precipitation, the land CO_2 fluxes are also influenced by atmospheric CO_2 concentrations and atmospheric nitrogen deposition. The NorESM2-LM model was not spun-up long enough, leading to a considerable preindustrial drift in the land carbon pools. We have therefore drift-corrected all changes in land carbon stocks presented here by estimating the trend at the end of the pre-industrial period in each gridcell and then removing the trend over all time series.

https://doi.org/10.5194/egusphere-2026-1673
Preprint. Discussion started: 8 April 2026

2.2.6 MPI-ESM1-2-LR

The land surface model of MPI-ESM1-2-LR, JSBACH3.20 includes components to describe the dynamics of terrestrial vegetation and the carbon cycle in interaction with the global climate (Mauritsen et al., 2019). Terrestrial vegetation in JSBACH includes a competition scheme for vegetation dynamics based on the productivity of woody and herbaceous plants (Brovkin et al., 2009). Vegetation dynamics are influenced by wildfires and anthropogenic fires simulated by the SPITFIRE model, which provides the area burned and carbon emissions to the atmosphere (Lasslop et al., 2014). The soil carbon model YASSO simulates the dynamics of four fast soil carbon pools, which differ for leaf and wood litter types, and one slow humus pool. YASSO simulates plausible soil density patterns with relative maxima in tropical and boreal forests, and the distribution is comparable to observations (Mauritsen et al., 2019). JSBACH3.20 did not include permafrost carbon, and the maximum soil carbon storage at high northern latitudes is not well captured by the model. Nitrogen and carbon pools are coupled based on CO_2-induced nitrogen limitation (Goll et al., 2017).

2.2.7 CNRM-ESM2-1

This study analyzes model outputs of CNRM-ESM2-2 (Bossert et al., 2025). Compared to its previous version (CNRM-ESM2-1, Séférian et al., 2019), CNRM-ESM2-2 offers an improved representation of the global carbon cycle, of several Earth system interactions (aerosols-light, biophysics, etc.) as well as an improved treatment of the anthropogenic disturbance on land.

The SURFEX v8.0 platform (Masson et al., 2013) is the surface component of CNRM-ESM2-1. It simulates surface state variables and fluxes at the surface-atmosphere interface, using the same grid and time step as the atmosphere model. It includes submodules for ocean, lake, and land surface types. Over land, ISBA-CTRIP models energy, water, and carbon budgets, solving soil heat and water transfer equations while accounting for soil organic carbon properties. It uses a 12-layer snow model, dynamic river flooding scheme, and groundwater dynamics (Decharme et al., 2019; Decharme and Colin, 2025).

ISBA-CTRIP represents the land carbon cycle by simulating plant physiology, carbon allocation, and soil carbon cycling (Delire et al., 2020). It includes modules for wildfires, land-use changes, and dissolved organic carbon transport to the ocean. Vegetation is modeled with 4–6 carbon pools depending on plant type, and 16 vegetation types are distinguished. Photosynthesis is represented by a semi-empirical model with a 10-layer radiative transfer scheme, while leaf phenology is driven by carbon balance. Soil carbon dynamics follow the CENTURY model (Parton et al., 1988), with four litter and six soil carbon pools releasing CO_2 through decomposition. Further details are provided in Decharme et al. 2019 and Delire et al. 2020. The version of ISBA-CTRIP included in CNRM-ESM2-2 accounts for harvesting process by using an agricultural module comparable to the one used in JULES (Osborne et al., 2015).

2.2.8 HadCM3LC-Bris

HadCM3LC-Bris is based on the HadCM3 climate model (Gordon et al., 2000), adapted for use with an interactive carbon cycle by adopting lower ocean resolution (Cox, 2001) and subsequently modified for use at University of Bristol (Valdes et al., 2017). The land carbon cycle is based on the MOSES-2 land surface model (Essery et al., 2003), with dynamic vegetation

https://doi.org/10.5194/egusphere-2026-1673
Preprint. Discussion started: 8 April 2026

which simulates phenology, growth and competition of five plant functional types (broad-leaved and needle-leaved trees, C3 and C4 grasses and shrubs). Soil carbon is represented in a single pool, with a "q10" dependence of decomposition on soil temperature.

2.2.9 UKESM1.2

UKESM1.2 is based on UKESM1.1 (Mulcahy et al., 2023) with the addition of interactive ice sheets over Greenland and Antarctica provided by the BISICLES model (Smith et al., 2021). The atmosphere model within UKESM1.2 is vn12.1 of the Met Office Unified Model, which is coupled to the NEMO ocean model. The land and ocean carbon cycle components of UKESM1.2 are essentially unchanged from UKESM1-0-LL (Sellar et al., 2019). The land surface scheme consists of the JULES land surface model (Clark et al., 2011; Harper et al., 2016), which includes 13 natural and 4 agricultural plant functional types, whose spatial distribution is determined by height-based competition via the TRIFFID dynamic vegetation model (Cox, 2001). Net primary productivity is limited by nitrogen availability (Wiltshire et al., 2021). Ocean biogeochemistry is provided by version 2.0 of the MEDUSA model (Yool et al., 2013).

2.2.10 MIROC-ES2L

The MIROC Earth system version 2 for long-term simulations (MIROC-ES2L; Hajima et al., 2020) is a model that was extensively used for the Coupled Model Intercomparison Project phase 6. The version used in this study is the same as that used for CMIP6 except for several bug fixes, and the spin-up was extended before performing the flat10-experiment. The land biogeochemical component is VISIT (Ito and Inatomi, 2012), which is interactively coupled to the land surface physics model (MATSIRO; Takata et al., 2003). The terrestrial biogeochemical component covers major processes relevant to the global carbon cycle, with vegetation (leaf, stem, and root), litter (leaf, stem, and root), and humus (active, intermediate, and passive) pools, under a static vegetation distribution. The nitrogen cycle is simulated with N pools consisting of vegetation (canopy and structural), organic soil (litter, humus, and microbe), and inorganic nitrogen (ammonium and nitrate).

2.3 Carbon pools

ESMs participating in flat10MIP report carbon content in either two or three land carbon pools. Within each ESM, carbon within each of these overarching pools may be represented by many more sub-pools, however at most only three pools are reported in the tier-1 C4MIP variables that form the basis for CMIP carbon cycle reporting (Jones et al., 2016). Three of the ESMs analyzed here report only vegetation and soil carbon pools (NASA-GISS-E2.1-G-CC2, UKESM1.2, HadCM3L-Bris), while the remaining ESMs report vegetation, soil, and litter pools. We analyze all three pools distinctly when available, as well as the sum of all land carbon pools within each ESM, which we report as total land carbon.

Internally within each model many more carbon pools may be represented. We report the number of soil carbon pools specifically (Table 1), noting the wide diversity in number of pools represented across ESMs, which range from 1 in HadCM3L-Bris to 7 within each of the 20 soil layers in CESM2 and NorESM2-LM, which results in a total of 140 soil carbon pools.

https://doi.org/10.5194/egusphere-2026-1673
Preprint. Discussion started: 8 April 2026

Table 1. Table of ESMs and relevant processes included in each

Model	Nutrient limitation	Vegetation Dynamics	Number of soil C pools	Reference
ACCESS-ESM1-5	N and P	LAI only	3	Ziehn et al. 2020
CESM2	N	LAI only	4 in each of 20 soil layers	Danabasoglu et al. 2020
GFDL-ESM4	none	height-age, PFTs, and LAI	4 in each of 20 soil layers	Dunne et al. 2020, Shevliakova et al. 2024
NASA-GISS-E2.1-G-CC2	none	plant labile and soil carbon (fixed LAI)	9	Romanou et al. 2026, Kim et al. 2015
NorESM2-LM	N	LAI only	4 in each of 20 soil layers	Seland et al. 2020
MPI-ESM1-2-LR	N	PFTs and LAI	9	Mauritsen et al. 2019
CNRM-ESM2-1	none	LAI only	6	Séférian et al. 2019, Delire et al. 2020
HadCM3LC-Bris	none	PFTs and LAI	1	Valdes et al. 2017
UKESM1.2	N	PFTs and LAI	4	Sellar et al. 2019
MIROC-ES2L	N	LAI only	6	Hajima et al. 2020

https://doi.org/10.5194/egusphere-2026-1673
Preprint. Discussion started: 8 April 2026

Of these ESMs, only CESM2, NorESM2-LM, and GFDL-ESM4 resolve soil carbon by depth (CESM2 and NorESM2-LM use CLM5 as their land component), which allows the separation of carbon in permanently frozen soil layers that may be thawed with warming from carbon that is actively cycling in shallow Arctic soils (Canadell et al., 2021, Table 5.4).

2.4 Nutrient limitation

Six of the ESMs analyzed here represent nutrient cycling and nutrient limitations to photosynthesis. ACCESS-ESM1-5 is the only ESM in this study that represents both phosphorous and nitrogen limitation. Five of the ESMs represent nitrogen limitation: NorESM2-LM, CESM2, MPI-ESM1-2-LR, UKESM1.2, and MIROC-ES2L.

2.5 Vegetation dynamics

All of the land surface components within the ESMs used in this study have prognostic carbon cycles, where carbon pools are updated over time in response to dynamically calculated fluxes. All but one of the ESMs represent prognostically calculated dynamic leaf area, where the area of leaves per area of ground is an emergent property of the carbon cycle, typically the leaf carbon pool. The exception is NASA-GISS-E2.1-G-CC2, where leaf area is specified from a dataset that varies seasonally within a year but not across years, and carbon uptake that would be allocated to stem growth is transferred as litterfall to the soil pools, leaving the prognostic land carbon pools to be the plant labile storage and soil carbon.

Natural vegetation, as opposed to vegetation changed by anthropogenic land use change, is specified in all of the ESMs represented here by discrete plant functional types. Plant types within a given gridcell are represented as either static in time or in some models as prognostically varying over time. Time-varying vegetation types are frequently referred to as "dynamic vegetation" (Cramer et al., 2001), although here we will use the term "dynamic biogeography" to differentiate variations in plant type from additional variations in plant age and size distributions. In GFDL-ESM4 plants are represented by cohorts of plant type and size-age, allowing for a more complex representation of ecosystem demographics and how they vary over time, which we term here a "demographic vegetation" model.

These various flavors of vegetation dynamics across models for leaf area, plant type, and plant demographics contribute to the timescales and behavior of land carbon storage and fluxes.

2.6 Analysis methods

We report averages for different time periods within the simulations as described in Section 2.1. We report zonal mean sums for three latitude bands: tropics ($20^o S$ to $20^o N$), mid-latitudes ($> 20^o$ and $< 50^o$), and high-latitudes ($> 50^o$), as well as full zonal profiles. These particular boundaries of each latitude zone were selected because they broadly represent transitions between higher and lower carbon stocks across ESMs. When multi-model mean values are reported in the text we include the multi-model standard deviation or range across ESMs in brackets.

https://doi.org/10.5194/egusphere-2026-1673
Preprint. Discussion started: 8 April 2026

3 Results and Discussion

3.1 Carbon stocks

3.1.1 Initial carbon stocks (pre-industrial state)

The IPCC 6th assessment report (AR6) estimates for pre-industrial carbon stocks are 450 PgC in vegetation, 1700 PgC in non permafrost soils, and 1200 PgC in permafrost soils, for a total global carbon budget estimate of 3350 PgC on land with 13% of carbon in vegetation (Canadell et al., 2021). The total estimated carbon in vegetation and soil excluding permafrost carbon reported by IPCC is 2150 PgC with 21% in vegetation (Canadell et al., 2021). Pre-industrial carbon stocks vary across ESMs in esm-flat10, both in total magnitude and in zonal distribution. The multi-model mean total global land carbon content is 1860 Pg [$\pm$568], with a range from the low end of 978 PgC in GFDL-ESM4 and a high of 3119 PgC in NorESM (Table A1).

Most of the ESMs have the majority of carbon in the soil rather than vegetation, with 30% [$\pm$8%] in vegetation and 63% [$\pm$13%] in soil (Table A1), and no model having less than 17% of carbon in vegetation. The relatively larger amount of carbon in soils compared with vegetation is consistent with other estimates of the global carbon cycle, however, the total magnitude of vegetation carbon pools is generally closer to the IPCC AR6 estimate, compared to the soil carbon pools. Overall, we find that a number of the ESMs have insufficient amounts of soil carbon relative to modern day observations (Fao, 2023; Jackson et al., 2017; Batjes, 2016; Hugelius et al., 2014; Canadell et al., 2021). In high latitudes specifically, a lack of sufficient carbon reflects that the representation of processes that govern carbon cycling in Arctic ecosystems is missing in most ESM soil models (Schuur et al., 2015, 2022; Natali et al., 2021; Matthes et al., 2025). Regional evaluation of CMIP6 models (Ito et al., 2020a; Jones et al., 2023) showed that there is a high diversity in performance across different regions and for different processes. Some models simulate fluxes better than pools and some vice versa. Some models perform well in some regions and poorly elsewhere. There were no clear "winners" in terms of models which performed well for all regions and all processes. It is likely the models used here, which are largely very closely related to CMIP6 versions, which exhibit a similar mix of skill across regions and processes.

Many ESMs have similar amounts of carbon in tropical ($< 20^o$) and mid-latitudes ($> 20^o$ and $< 50^o$) relative to high latitudes ($> 50^o$), with the notable exception of NorESM which has a very large high latitude carbon soil carbon pool. CESM2 has more high latitude carbon than mid latitude carbon, but not nearly to the same degree as NorESM despite these two models using the same land carbon cycle representation (Fig. 2a-c, 4, 5, Table A2).

https://doi.org/10.5194/egusphere-2026-1673
Preprint. Discussion started: 8 April 2026

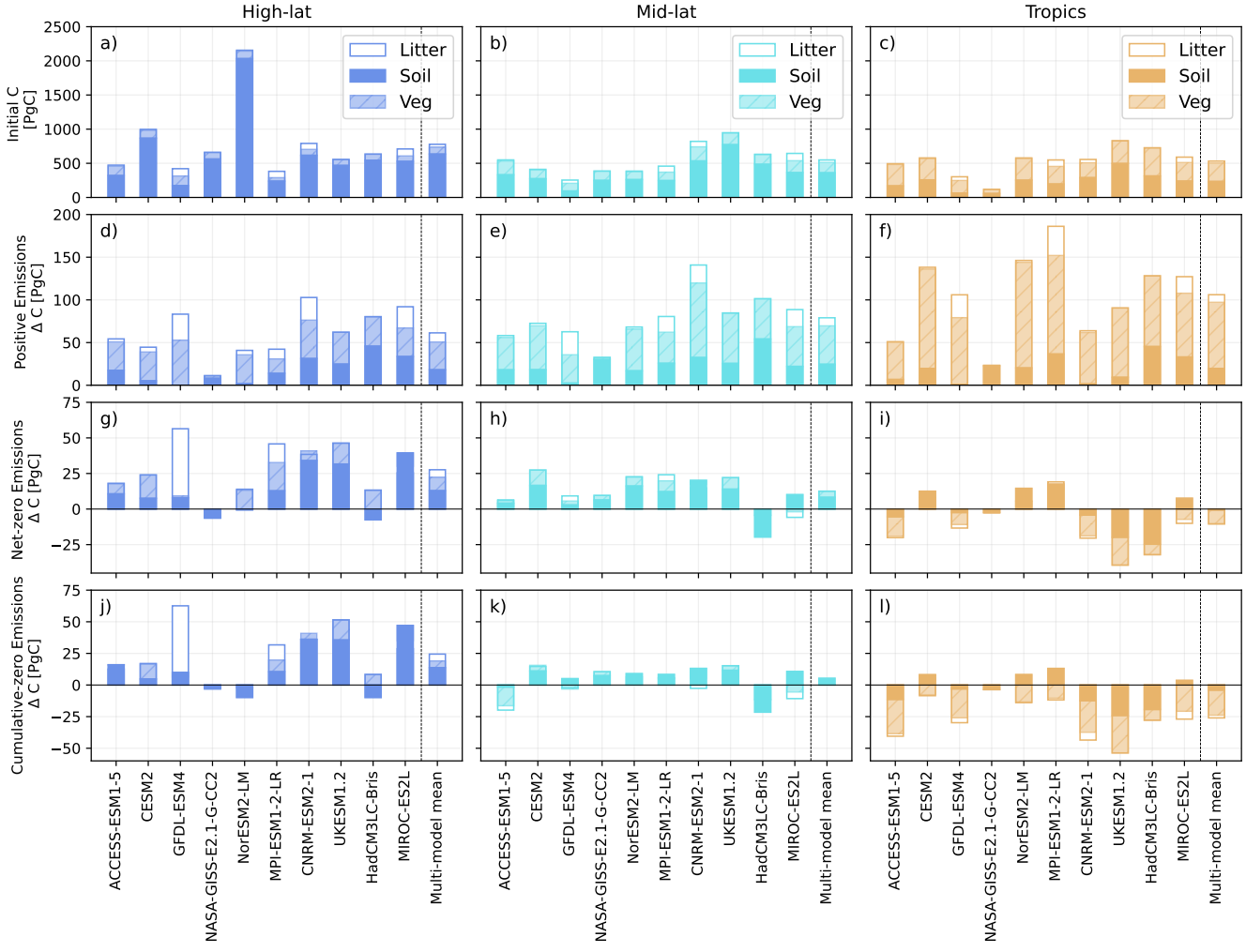

Figure 2. Carbon and Δcarbon at different latitudes. Bar graph showing initial carbon stocks (first row), and change in carbon stocks after positive emissions phase (second row), after net-zero emissions (third row), and after negative emissions emissions (fourth row) in each of the ESMs participating in flat10MIP. Each column shows the initial stock or change in C for soil carbon (solid dark color), vegetation carbon (lighter color), and litter (white with outline) high-latitudes ($> 50^o$) in the left column, mid-latitude regions ($> 20^o$ and $< 50^o$) in the middle column, and tropical regions ($< 20^o$) in the right column.

https://doi.org/10.5194/egusphere-2026-1673
Preprint. Discussion started: 8 April 2026

In the tropics ESMs simulate a large fraction of carbon in vegetation, with increasing relative amounts of soil carbon at mid to high latitudes. Across all ESMs in mid-latitudes carbon stocks are >50% in soil (except for GFDL-ESM4) and in high-latitudes carbon is mostly in soil (76 % [±14%]), Fig. 4, 5).

The variation in global vegetation, litter and soil stocks across models are substantial (Fig. 2a-c). Given that soil and vegetation stocks require long spin-up and historical transient runs to reach a state which is comparable with present day observations, they are among the most challenging of targets for model calibration. This plausibly explains the wide variation of initial carbon stocks. Different initial carbon stocks imply potentially different vulnerability to change – vegetation is typically represented as having a faster turnover time relative to soils. Thus an ESM with a larger fraction of carbon stored in vegetation could lose carbon more quickly compared to an ESM with relatively more carbon stored in soils.

https://doi.org/10.5194/egusphere-2026-1673
Preprint. Discussion started: 8 April 2026

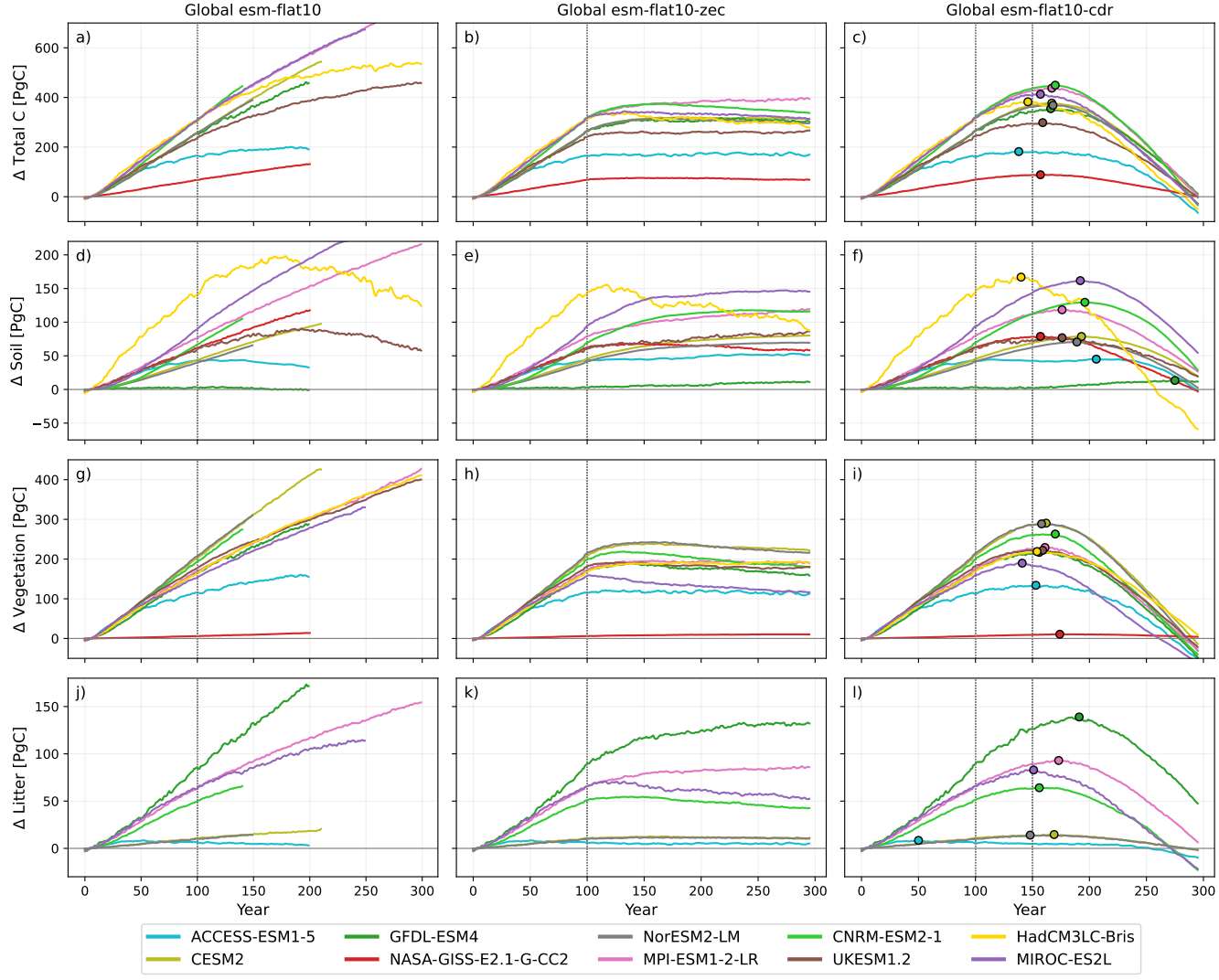

Figure 3. Global mean timeseries of carbon pools Time series of global mean change in carbon stocks in each of the ESMs participating in flat10MIP in units of PgC with total carbon in the top row, soil carbon in the second row, and vegetation carbon in the third row, and litter carbon in the fourth row (not all ESMs report litter). Columns show each of the three experiments: esm-flat10 (left), esm-flat10-zec (middle), and esm-flat10-cdr (right). Each line represents one ESM. Colored circles indicate the year of peak carbon stock during the esm-flat10-cdr experiment.

https://doi.org/10.5194/egusphere-2026-1673
Preprint. Discussion started: 8 April 2026

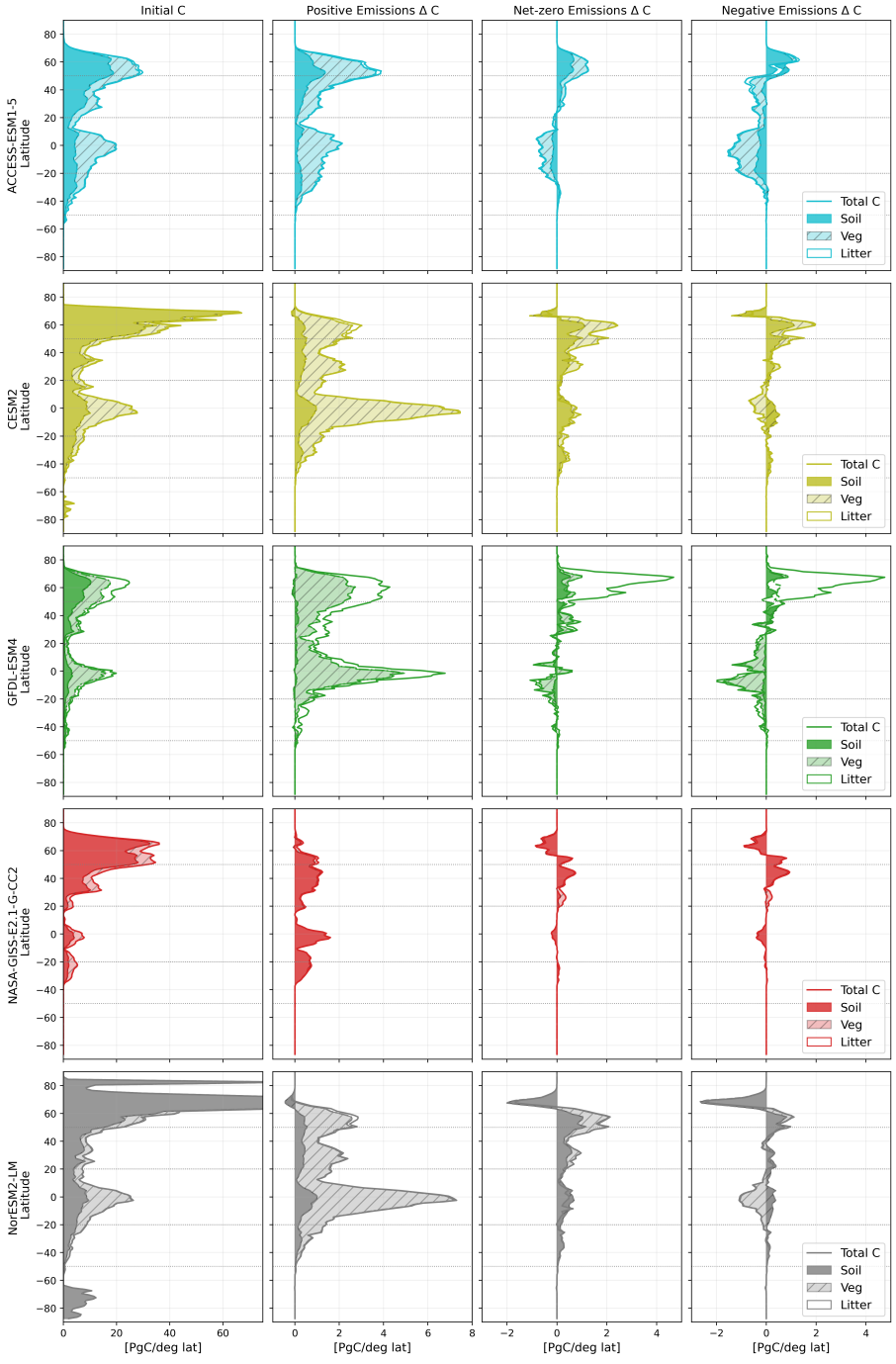

Figure 4. Initial C and ΔC at each emissions phase. Zonal initial carbon stocks and change in carbon stocks (columns) for a subset of the ESMs participating in flat10MIP (rows) in units of PgC (remaining ESMs shown in Fig. 5) with one ESM shown on each row. The left column shows initial carbon stocks, the second from left column shows the end of the positive emissions phase, third from left column shows the net-zero phase, and right column shows the point of cumulative-zero emissions relative to the initial carbon pools. Total carbon pool is shown with a solid line, soil carbon pool in the dark shaded area, vegetation carbon pool in the light hatched area, and litter carbon in white. Dashed lines indicate 50^o and 20^o North and South.

https://doi.org/10.5194/egusphere-2026-1673
Preprint. Discussion started: 8 April 2026

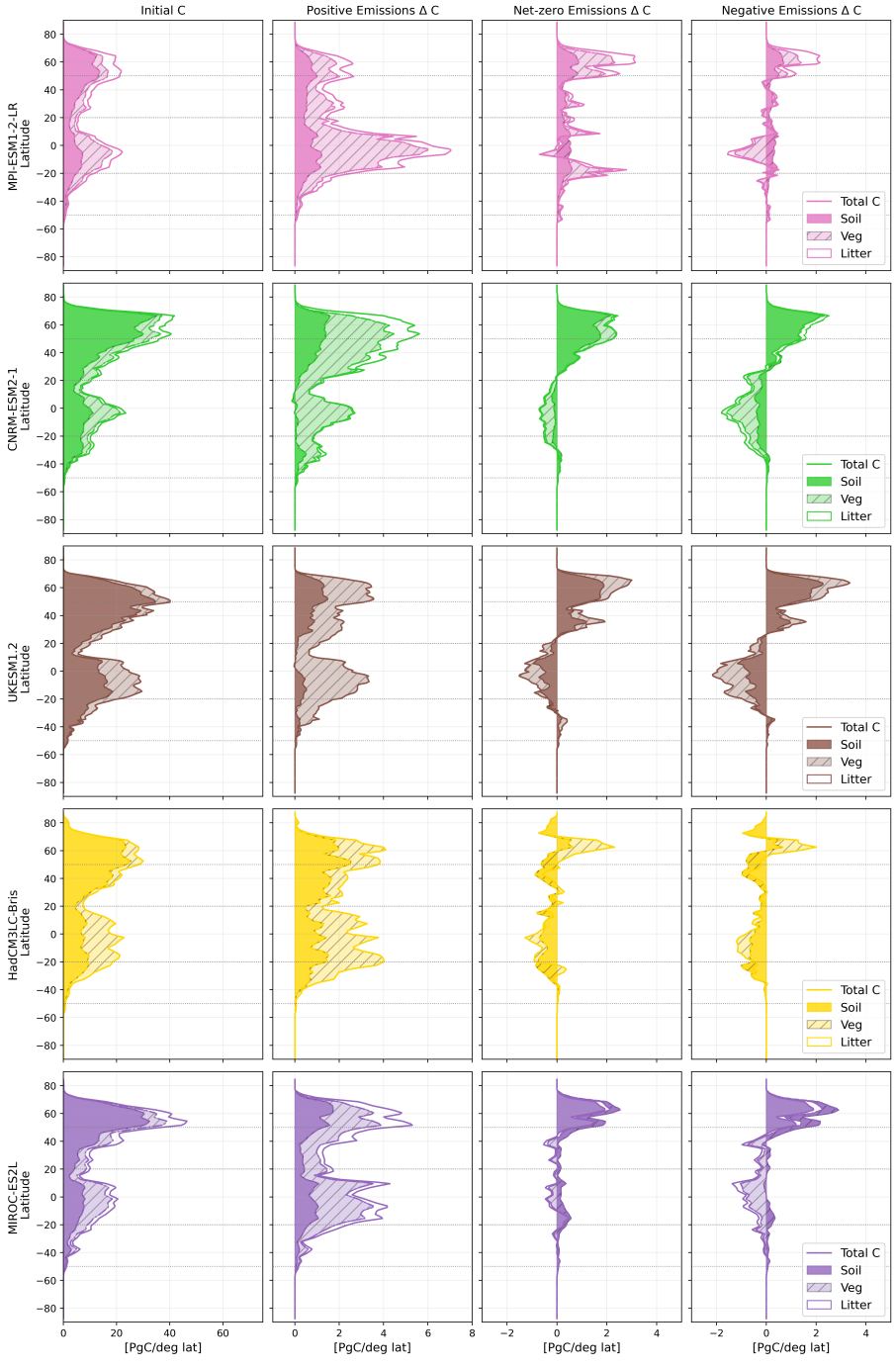

Figure 5. Initial C and ΔC at each emissions phase. The same as in Figure 4 for the remaining ESMs.

https://doi.org/10.5194/egusphere-2026-1673
Preprint. Discussion started: 8 April 2026

3.1.2 Positive Emissions phase (esm-flat10)

During the positive emissions phase of the esm-flat10 experiment, CO_2 is emitted to the atmosphere at 10 PgC/yr for 100–300 years, depending on the ESM. As a result, CO_2 accumulates in the atmosphere (Fig. 1g), with land and ocean sinks together removing about half of the emissions (Sanderson et al., 2025). Global mean surface temperatures increase as a result of the radiative forcing from elevated CO_2 and associated climate feedbacks (Fig. 1j). During this phase of increasing atmospheric CO_2 and increasing temperature, land carbon pools increase in all models (multi-model mean increase of 246 PgC [$\pm 71 Pg$] globally at year 100), with the additional carbon being primarily added to vegetation pools (60% [$\pm$19%]) (Table A1).

Elevated CO_2 conditions generally enhance photosynthesis (Farquhar et al., 1980), the basic process for which is represented in all of these ESMs. During the positive emissions phase temperatures are increasing, but may not have yet reached temperatures hot enough to inhibit photosynthesis either directly (Mathur et al., 2014) or indirectly (Grossiord et al., 2020; Zarakas et al., 2024). Enhanced photosynthesis first increases carbon (C) flux into live vegetation pools and is only transferred to litter or soil pools after some time, a pattern which is shown consistently across ESMs (Fig. 2). Gains in carbon in the first 100 years occur primarily in vegetation (between 50% and 81% excluding NASA-GISS-E2.1-G-CC2) and are largest in the tropics and mid-latitudes (Fig. 2).

The first 100 years of 10 PgC/yr emissions results in a total emission of 1000 PgC into the atmosphere. This 1000 PgC mark is the point at which climate metrics like the transient climate response to CO_2 emissions (TCRE) are calculated (Sanderson et al., 2025). All ESMs show an increase in total carbon stocks during the first 1000 PgC of emissions, however ACCESS-ESM1-5 exhibits slightly different behavior compared to the other ESMs. As cumulative emissions increase it is the first ESM to have carbon pools that grow at less than a linear rate starting at around 500 PgC of cumulative emissions (year 50), which is most prominent in the tropics, and occurs in both soil and vegetation (Figs. 3, Fig. A3).

Most ESMs extended their simulations with constant emissions past 100 years to higher levels of cumulative emissions as was requested in the flat10MIP experimental design (Sanderson et al., 2025). Carbon accumulates on land nearly linearly for the first 100 years in most models, and this linearity could be used for simplification of the climate-carbon dynamics (Brovkin et al., 2025). The accumulation rate slows for a few ESMs at higher cumulative emissions (Fig. 3), but many continue accumulating carbon on land at a near-linear rate all the way to 3000 PgC of cumulative emissions. The deviation from a linear increase in carbon pools with cumulative emissions seen in some ESMs (ACCESS-ESM1-5, HadCM3LC-Bris, UKESM1.2) occurs in both vegetation pools and soil pools, with noticeable peaks followed by declines in soil carbon, driven primarily by large declines in tropical soil carbon and plateauing of tropical vegetation carbon (Figs. 4, 5, A3). Vegetation carbon does not decline in any ESM during the positive emissions phase, but grows less than linearly in many ESMs after year 100. In ACCESS-ESM1-5 , tropical GPP begins to saturate by year 100 and then declines slightly, leading to a tapering off of increases in global GPP (Fig. A4). ACCESS-ESM1-5 is the only ESM analyzed here that includes both nitrogen and phosphorous limitation, but nutrients are not the only constraints on vegetation growth, and GPP in the tropics in particular is limited by hot temperatures in combination with faster vegetation turnover. Vegetation carbon also saturates in HadCM3C-Bris and UKESM1.2 after year 100, however this tapering off is not driven by GPP (Fig. A4), and instead must be occurring due to faster turnover of vegetation

https://doi.org/10.5194/egusphere-2026-1673
Preprint. Discussion started: 8 April 2026

carbon pools. Across ESMs we see no association between the continued rate of accumulation of land carbon with cumulative emissions and representation of nutrient limitation. The ESMs with low (ACCESS-ESM1-5) and the highest (MIP-ESM1-2-LR, MIROC-ES2L) as well as intermediate levels (UKESM1.2, CESM2, NorESM2-LM) of accumulation all have dynamic representation of nutrient limitation.

Satellite remote sensing based observations of recent decades (Xu et al., 2021) suggest that above ground biomass has not accumulated as quickly as ESMs project (Randerson et al., 2025; Bar-On et al., 2025). Two possible hypotheses have been presented in the literature. The first hypothesis is that the total land sink estimate is broadly correct and therefore gains in soil carbon have been proportionally larger than gains in above ground carbon that is visible to remote sensing (Bar-On et al., 2025). The second hypothesis is that the relative amount of above and below ground carbon remained stable and therefore the total land carbon sink must be weaker than previously thought, which can be reconciled with global scale constraints by corresponding adjustments to estimates of ocean sinks and anthropogenic emissions (Randerson et al., 2025). Overall, the ESMs analyzed here show relatively larger gains in vegetation vs. soil carbon during the positive emissions phase (Table A1). NASA-GISS-E2.1-G-CC2 is an outlier showing an increase at the end of the positive emissions phase of only 67 PgC, occurring 90% in soil carbon pools, making its response more consistent with the first hypothesis. By contrast, ACCESS-ESM1-5 has the next lowest accumulation of land carbon yet gained 2.4 times more carbon on land than NASA-GISS-E2.1-G-CC2 (Table A1) and no other ESM had less than 50% of additional carbon added to vegetation pools. We note that the flat10MIP simulations are idealized and do not account for specific factors such as land use change that are needed for direct comparison with observed land carbon accumulation during the historical period. However the land model components of many of the ESMs participating in flat10MIP are also used to make estimates of the historical period through comparisons such as those used by the Global Carbon Project (Friedlingstein et al., 2025). Although overall Randerson et al. (2025) report that many ESMs show larger accumulation of vegetation carbon than is indicated by remote sensing based estimates, we note that for three of the ESMs analyzed here, the closest relatives show accumulation rates similar to observations (ACCESS-ESM1-5, MPI-ESM2-2-LR, UKESM1.2, Randerson et al., 2025).

Although ESMs generally agree that vegetation carbon will increase during the positive emissions phase, important mechanisms limiting vegetation growth may not be adequately represented in ESMs (see further discussion below).

3.1.3 Net-zero (esm-flat10-zec)

During the net-zero phase, carbon global stocks remain elevated above the end of the positive emissions phase in most models (Fig. A1, exception HadCM3LC-Bris). Carbon gain occurs in nearly all models in mid- and high-latitudes (Fig. 2c, A2), largely in soil carbon pools (Fig. 2). Carbon is lost in tropical latitudes in most models, and vegetation carbon declines in tropical latitudes in all models (Fig. 2, Table A2).

As time under net-zero emissions progresses (year 100-300 in esm-flat10-zec), land and ocean carbon sinks continue to draw down CO_2 from the atmosphere, leading to a decrease in atmospheric CO_2 concentrations. Carbon loss in the tropics occurs (Fig. 2, A3) as the fertilization effect of elevated atmospheric CO_2 partially reverses, while temperatures remain high causing faster respiration rates and potentially higher plant stress in hot places. In higher latitudes, carbon stocks are flat or

https://doi.org/10.5194/egusphere-2026-1673
Preprint. Discussion started: 8 April 2026

increasing in most models for vegetation and soil, with the exception of carbon loss from high latitude soils in NorESM2-LM, NASA-GISS-E2.1-G-CC2, and HadCM3LC-Bris (Figs. 2,A2, A1).

In HadCM3LC-Bris we see both a larger gain in soil carbon during the emissions phase and a greater loss of soil carbon in the tropics and mid-latitudes, leading to an overall decline in carbon stocks during net-zero emissions (Fig. 4, 5). This is not driven by higher temperatures compared to other models, as HadCM3LC-Bris has a TCRE close to the median, or by differences in photosynthetic response to elevated CO_2 and temperature. Instead, it is likely to be driven by a structural feature of single-pool soil carbon models. Jones et al 2005 show that a single soil carbon pool is constrained to follow much more rapid response timescales than a multi-pool model. The soil carbon itself is not more sensitive to temperature, but simply the timescale to realize the response is much shorter. This represents a possible failing of older generation models like HadCM3, as it affects the timescale to approach a longer-term response if not the longer-term response itself (Fig. 3).

3.1.4 Negative and cumulative zero emissions (esm-flat10-cdr)

The end of the flat-10-cdr experiment represents the point of zero cumulative emissions. Here we compare the point of cumulative zero emission (year 300) to the initial pre-industrial state to evaluate the reversibility of carbon pools under negative emissions, which we call "cumulative-zero emissions". We note that at the point of cumulative-zero the system is not yet in equilibrium, so we are comparing this transient state with the initial state of the system.

At cumulative-zero emissions, carbon has been lost from vegetation in most ESMs, and from the tropics in all ESMs (Figs. 2, A2). This also applies to soil carbon in many models (Fig. 4, 5). Many ESMs show gains in total carbon in the mid-latitudes due to increases in soil carbon (except for HadCM3LM-Bris), and in the high-latitudes due to increases in both soil carbon and vegetation carbon (Fig. 2).

Although the zonal profiles of carbon pool response at net-zero and at cumulative-zero appear similar in terms of which latitudes and pools are gaining or losing carbon, these responses are taking place at different mean states of carbon. During the period of net-zero emissions carbon pools are adjusting from their elevated state at the end of the positive emissions phase, resulting in losses from that state but overall higher stocks (Fig. 3). In contrast, after negative emissions at the point of cumulative-zero emissions carbon pools have had a similar scale of response, but the perturbation is relative to their lower carbon pre-industrial state. The similarity between these two responses (following net-zero and at cumulative-zero emissions) suggests that similar processes are acting on carbon pools, although with different magnitudes and rates.

3.2 Tropical carbon vulnerability

All of the ESMs show loss of tropical vegetation carbon during a period of net-zero emissions, as well as following negative emissions at cumulative-zero emissions. During the positive emissions phase, GPP increases and carbon is gained on land, and in the tropics this is likely due primarily to CO_2 fertilization enhancing growth- either directly through higher rates of photosynthesis, or indirectly through increased water use efficiency (Fig. 4, 5, A4j). A few ESMs show either less-than-linear growth or tapering off of vegetation carbon with positive emissions that exceed $1000 PgC$ (year 100). Tropical carbon begins to degrade, however, during both the net-zero phase and under negative emissions, due to saturation of vegetation carbon

https://doi.org/10.5194/egusphere-2026-1673
Preprint. Discussion started: 8 April 2026

pools and losses from soils (Fig. A3). This suggests that the effect of hotter temperatures, and fast response to declining CO_2 concentrations, experienced over this period outweighs any delayed fertilization effects from the period under which CO_2 concentrations were increasing.

This loss of tropical carbon under sustained hot temperatures with declining atmospheric CO_2 is occurring in these ESMs despite the lack of representation of many important processes that may further limit tropical vegetation productivity in a hotter world.In particular ESMs are missing representation of heat stress damage including impacts on enzyme functioning, reproduction, growth, and mortality (Jagadish et al., 2021; Bita and Gerats, 2013; Haberstroh et al., 2022), disturbance associated with fire (Canadell et al., 2021, Table 5.4), and changes in plant mortality rates including from hydraulic stress, pests, and pathogens (Allen et al., 2015; Bennett et al., 2015; Gazol and Camarero, 2022; Gazol et al., 2025; Hartmann et al., 2022; McDowell et al., 2022; Phillips et al., 2010; Senf et al., 2020). Together these mechanisms would tend to decrease vegetation carbon uptake, with potentially large magnitude losses which could occur abruptly. Thus the declines in carbon in these ESM simulations are likely to be an underestimate of the full effect of prolonged hot temperatures on terrestrial carbon storage in the tropics.

3.3 Mid- and high-latitude soil and permafrost carbon stocks

All but one ESM show gains in mid-latitude carbon pools, and most ESMs show gains in high latitude soil carbon pools after net-zero emissions (Fig. 4, 5). This is also true after negative emissions at cumulative-zero emissions (Fig. 2). This increase in soil carbon is consistent with the carbon gains that would be achieved by warming enhanced photosynthesis (Fig. A4) being transferred into soil pools over time.

Three of the ESMs analyzed here resolve soil carbon by depth which allows for the representation of permafrost soils. Two of the ESMs that include permafrost processes have high initial permafrost soil carbon stocks (CESM2 and NorESM2-LM, both of which use the same land surface model) and also show stagnation or losses from the high-latitude soil carbon pool during the zero emissions phase, reflective of the response to elevated temperatures driving permafrost carbon losses (Fig. A1). This permafrost carbon loss response is also consistent with results from a permafrost-enabled ensemble of UVic_ESM (MacDougall, 2021) that showed a wide and poorly-constrained range of potential permafrost carbon losses under zero emissions. The third ESM (GFDL-ESM4) shows low initial stocks of high latitude soil carbon suggesting a lack of permafrost representation despite vertically resolved soil carbon pools.

3.4 Timing of peak land carbon

During the period of declining and then net-negative emissions, CO_2 in the atmosphere peaks and then declines. This occurs due both to the reduction in emissions, as well as from land and ocean sinks continuing to draw down carbon for some time. This rate of land as well as the rate of ocean sink determines the atmospheric CO_2 concentration, which subsequently causes radiative forcing. ZEC is governed by an emergent tradeoff between warming caused by excess radiative forcing due to airborne emissions of CO_2 that have not been taken up by land or ocean sinks and the rate of ocean heat uptake. Thus we expect ZEC to be influenced by both the magnitude of total carbon sinks out of the atmosphere and the rate at which those sinks occur. On land, those sinks are determined by processes controlling timescales of carbon loss from vegetation and soils.

https://doi.org/10.5194/egusphere-2026-1673
Preprint. Discussion started: 8 April 2026

Peak atmospheric CO_2 concentration occurs before the point of net-zero emissions owing to these land and ocean sinks (-15 years [±7], Fig. 6f). Temperature, which is responding to the transient changes in radiative forcing from CO_2 and associated radiative feedbacks as well as the rate of ocean heat uptake, peaks at -6 years [±12] relative to the year of net-zero emissions (Fig. 1l).

Under these conditions of peaking and then declining atmospheric CO_2 concentrations and elevated temperatures, photosynthesis also peaks and then declines, leading to reductions in vegetation pools first, followed by litter and soil pools (Fig. 3). Vegetation carbon peaks 10 years [±7] after the point where net-zero emissions is reached (Fig. 6b). This relatively consistent pattern suggests some degree of homogeneity across ESMs in the processes controlling vegetation growth and decay, resulting in consistent timescales of behavior. Vegetation carbon peaks prior to net-zero emissions in some ESMs in the tropics, but after net-zero in all ESMs in mid- and high-latitudes (Fig. A5 second row). Overall, the peak in total carbon largely reflects the peak in vegetation carbon across all latitude regions (Fig. A5).

Soil carbon exhibits a much broader range of behavior in time, with peak soil carbon occurring on average 33 years after net-zero emissions, but with a range between -9 years and 126 years relative to the year of net-zero emissions (Fig. 6d). HadCM3LM-Bris shows peak global soil carbon before net-zero, which is driven by loss of mid-latitude soil carbon that precedes net-zero (Fig. A5 fourth row). On the longest end of the range for lagged responses, GFDL-ESM4 shows a very late peak of soil carbon at 126 years following net-zero. This is likely owing to the structural differences in GFDL-ESM4's representation of soil carbon which decreases soil turnover time as net primary production increases Sulman et al. (2014). Peak global soil carbon for most ESMs occurs 27-57 years after the year of net-zero emissions, a signal which is dominated by the peak in mid- and especially high-latitude soil carbon pools, as tropical soil carbon peaks more than 40 years before net-zero in many ESMs (Fig. A5). This spread in peak global soil carbon represents a substantial spread relative to timing of peak vegetation carbon at all latitudes, consistent with what has been found in prior analyses by Ito et al. 2020a.

https://doi.org/10.5194/egusphere-2026-1673
Preprint. Discussion started: 8 April 2026

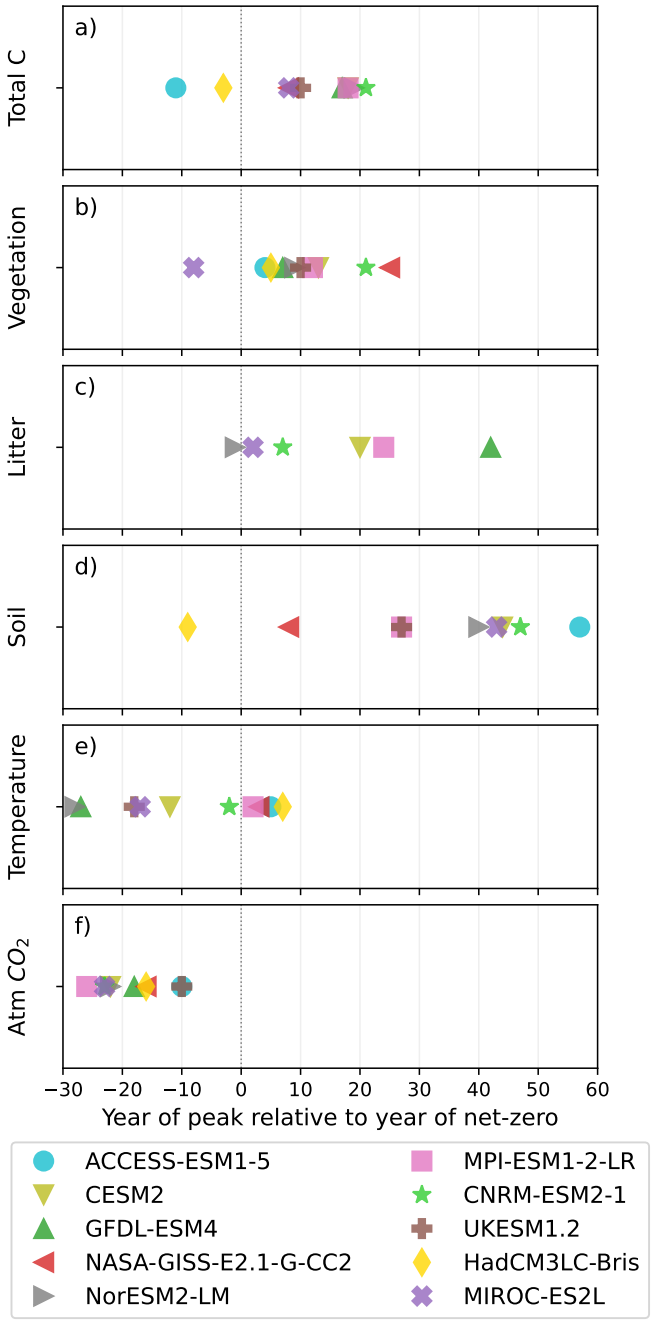

Figure 6. Year of peak relative to year of net-zero. Each panel shows the year at which that variable reaches its maximum value relative to the year in which emissions reach zero in the esm-flat10-cdr experiment. Each of the ESMs participating in flat10MIP is represented by one symbol. Rows show (from top) total carbon, vegetation carbon, litter carbon, soil carbon, globally averaged near surface temperature, and globally averaged atmospheric CO_2 concentration.

https://doi.org/10.5194/egusphere-2026-1673
Preprint. Discussion started: 8 April 2026

3.5 Unresolved structural and parametric uncertainty

The first set of flat10MIP simulations (Sanderson et al., 2025) have a range of TCRE across the ensemble of 1.32 $K/1000PgC$, with TCRE values across ESMs ranging from 1.18 to 2.50. However, the multi-model ensemble may underestimate the potential range of land carbon cycle uncertainty, due to lack of process understanding and parametric uncertainty. Slight variations in land parameter assumptions in a perturbed parameter ensemble that varied assumptions only about land processes (Booth et al., 2012) show a range of TCRE of 2.2 $K/1000PgC$ within a single model, with TCRE values from 1.57 to 3.77. Thus a single ESM has the potential to generate a wide range of TCRE, and possibly ZEC as well, due to different rates of carbon sinks alone, and this structural and parametric uncertainty has not yet been sampled.

4 Conclusions and Implications

ESMs participating in flat10MIP have a wide range of magnitude of pre-industrial carbon stocks. They additionally disagree on the zonal distribution of carbon as well as the partitioning between vegetation and soil carbon. ESMs in this study have been used in emissions-driven simulations, which by definition prognostically calculate atmospheric CO_2 as an emergent balance between sources (of which human emissions are specified) and sinks calculated within the ESMs. Given that many of these ESMs have been used to simulate the historical period, these ESMs can be compared against observed historical trajectories of atmospheric CO_2 (Hajima et al., 2025). Observations of atmospheric CO_2 carbon stocks, made through measurements of atmospheric CO_2 mixing ratio, are far more precise than observational estimates for either land or ocean stocks, and particularly for the zonal distribution of such stocks. While it is theoretically possible that ESMs could have tuned their emergent total land carbon stocks to match observationally-based estimates, it is highly unlikely that ESMs did so, given the high computational cost and considerable uncertainty associated with the best estimates of land and ocean carbon stocks.

Although the wide range of simulated pre-industrial carbon stocks across the ESMs we analyze here are therefore not a surprise, this spread still has implications for the subsequent behavior of land carbon sinks. Recent assessments of the offline properties of the present set of global land surface schemes indicates that large ranges in predicted soil and vegetation carbon remain (Friedlingstein et al., 2025). Refinements in the simulation of vegetation growth processes that allow more detailed constraints on vegetation growth rate, turnover and structure via consideration of vegetation demography, may help narrow the range of model predictions moving forwards.

Our findings here highlight that tropical carbon is most likely to be both gained and subsequently lost under positive, zero, declining, and negative emissions. This creates possible headwinds for carbon dioxide removal through afforestation and reforestation, the majority of which is projected to be implemented in low latitudes (Griscom et al., 2017; Cook-Patton et al., 2020; Mo et al., 2023). The esm-flat10-cdr simulations impose the magnitude of the carbon dioxide removal as a boundary condition of the emissions-driven scenario through a negative emissions flux - they do not actually model the processes driving carbon dioxide removal itself some of which could have additional climate impacts due to physical changes to the land surface (i.e. Swann et al., 2012; King et al., 2024). In reality, our ability to remove CO_2 from the atmosphere, in particular through

https://doi.org/10.5194/egusphere-2026-1673
Preprint. Discussion started: 8 April 2026

reforestation or afforestation, is likely to be negatively affected by the same adverse conditions for carbon storage that provoke the loss in tropical carbon stocks in these scenarios.

Timescales associated with vegetation carbon, as measured by the timing of peak vegetation carbon relative to the time of net-zero emission under the esm-flat10-cdr scenario, are relatively consistent across ESMs and across latitudes (Fig. 6, A5). Soil carbon timescales, on the other hand, vary widely across ESMs at all latitudes. The disagreement between both soil initial states and soil response timescales highlights greater structural uncertainty associated with soil carbon pools, as well as the challenge associated with assessing the behavior of a slowly evolving pool.

The wide variation across ESMs in soil carbon responses, which set the longest timescale of terrestrial carbon cycle response, has important implications for the role of terrestrial carbon cycle uncertainties for influencing ZEC. ZEC is an emergent property of the Earth system that captures the decadal- to century-timescale adjustment of temperature following net zero emissions. It emerges as a balance between the slowing of ocean heat uptake balanced by reductions in radiative forcing from CO_2 as land and ocean sinks draw carbon out of the atmosphere. Timescale responses longer than decades are particularly important in setting ZEC, and thus the response of soil carbon pools on land, as well as ocean carbon uptake, are likely to be more important for ZEC than vegetation carbon timescales. Given the lack of agreement across the ESMs analyzed here on the timing of soil carbon response, constraining ZEC from ESM behavior remains a challenge, and highlights the urgent need to better understand and simulate soil carbon processes.

Code and data availability. Data and analysis scripts are published at https://doi.org/10.5281/zenodo.19197571

https://doi.org/10.5194/egusphere-2026-1673
Preprint. Discussion started: 8 April 2026

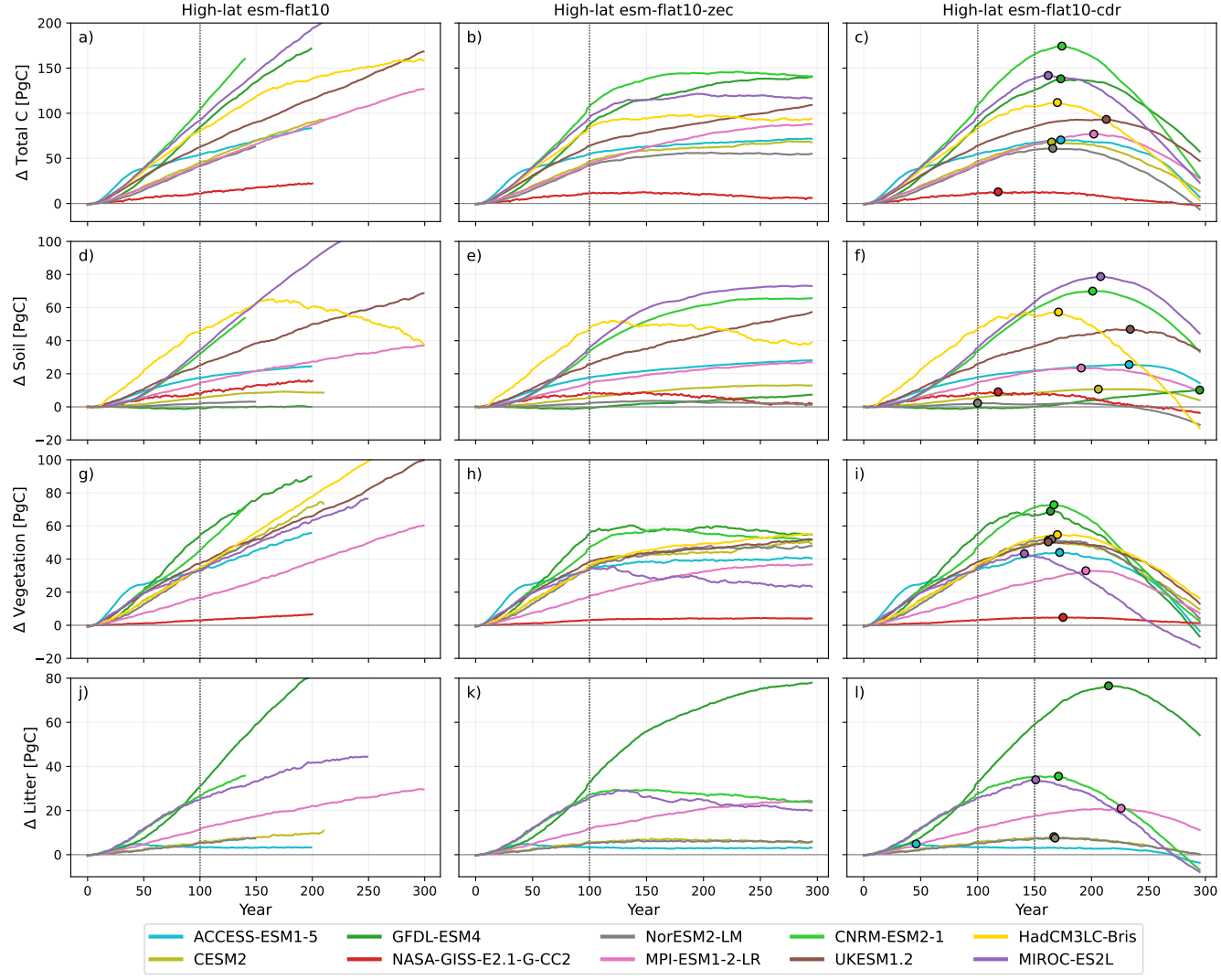

Figure A1. Timeseries of carbon pools for high-latitudes. Time series of change in carbon stocks in high-latitudes in each of the ESMs participating in flat10MIP in units of PgC with total carbon in the top row, soil carbon in the second row, and vegetation carbon in the third row, and litter carbon in the fourth row (not all ESMs report litter). Columns show each of the three experiments: esm-flat10 (left), esm-flat10-zec (middle), and esm-flat10-cdr (right). Each line represents one ESM. Colored circles indicate the year of peak carbon stock during the esm-flat10-cdr experiment.

https://doi.org/10.5194/egusphere-2026-1673
Preprint. Discussion started: 8 April 2026

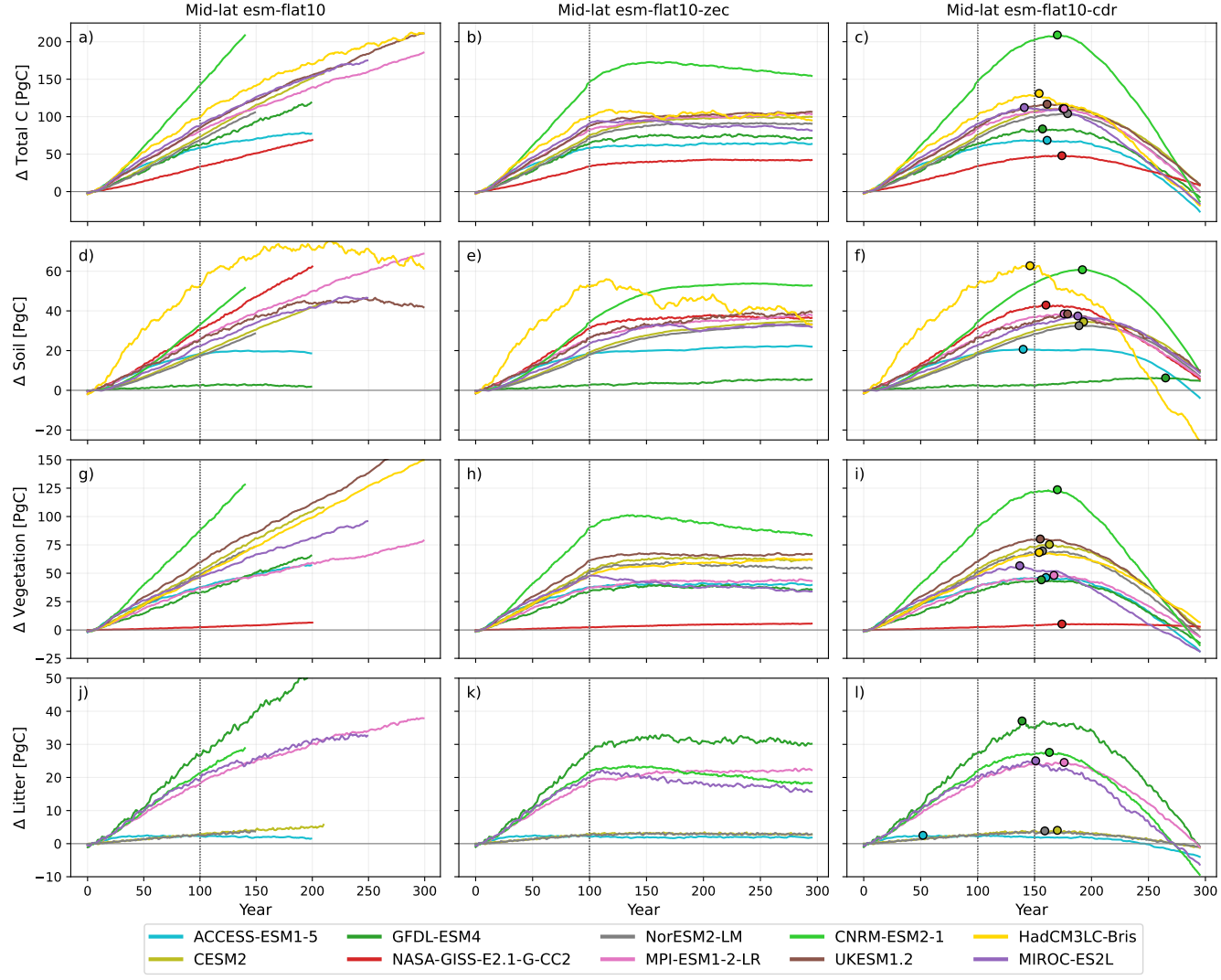

Figure A2. Timeseries of carbon pools for mid-latitudes. Time series of change in carbon stocks in mid-latitudes in each of the ESMs participating in flat10MIP in units of PgC with total carbon in the top row, soil carbon in the second row, and vegetation carbon in the third row, and litter carbon in the fourth row (not all ESMs report litter). Columns show each of the three experiments: esm-flat10 (left), esm-flat10-zec (middle), and esm-flat10-cdr (right). Each line represents one ESM. Colored circles indicate the year of peak carbon stock during the esm-flat10-cdr experiment.

https://doi.org/10.5194/egusphere-2026-1673
Preprint. Discussion started: 8 April 2026

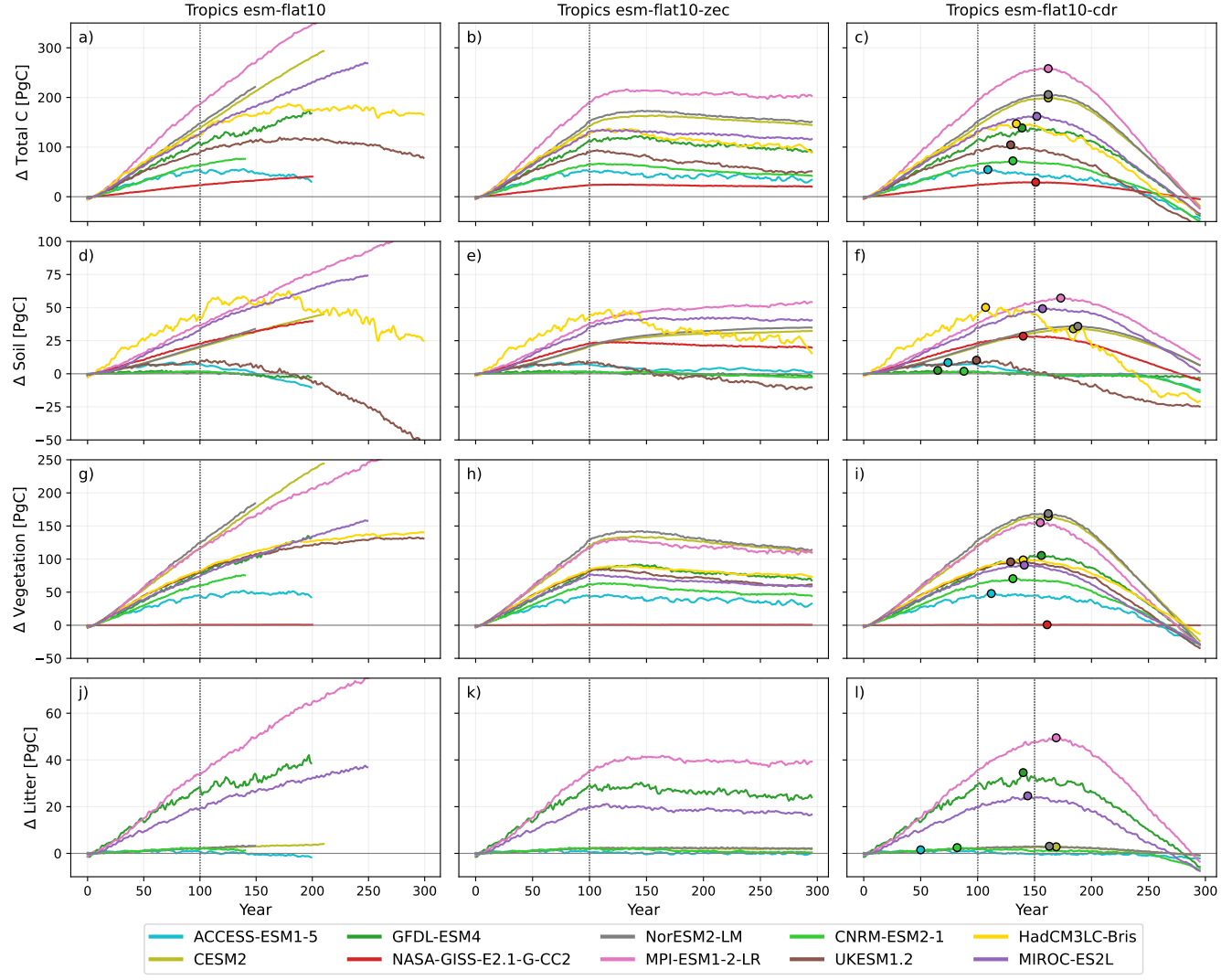

Figure A3. Timeseries of carbon pools for tropical latitudes. Time series of change in carbon stocks in tropical latitudes in each of the ESMs participating in flat10MIP in units of PgC with total carbon in the top row, soil carbon in the second row, and vegetation carbon in the third row, and litter carbon in the fourth row (not all ESMs report litter). Columns show each of the three experiments: esm-flat10 (left), esm-flat10-zec (middle), and esm-flat10-cdr (right). Each line represents one ESM. Colored circles indicate the year of peak carbon stock during the esm-flat10-cdr experiment.

https://doi.org/10.5194/egusphere-2026-1673
Preprint. Discussion started: 8 April 2026

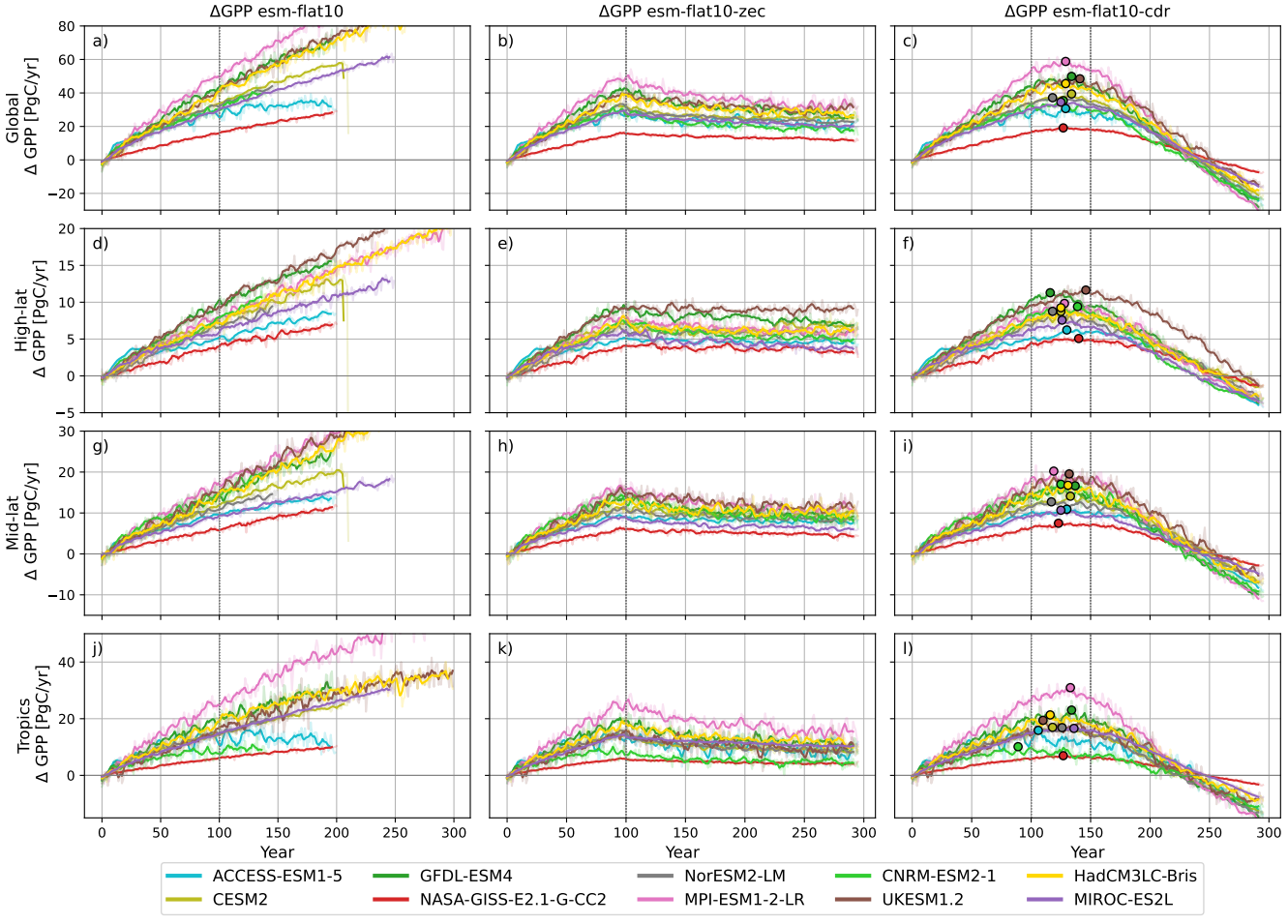

Figure A4. Timeseries of GPP for different latitudes. Time series of change in GPP at different latitudes in each of the ESMs participating in flat10MIP in units of PgC with the global average in the top row, high-latitude average in the second row, mid-latitude average in the third row, and tropical average in the bottom row. Columns show each of the three experiments: esm-flat10 (left), esm-flat10-zec (middle), and esm-flat10-cdr (right). Each color represents one ESM. Light shaded lines show the full interannual variability and soild colored lines have been smoothed with a 5 year running mean. Colored circles indicate the year of peak carbon stock during the esm-flat10-cdr experiment.

https://doi.org/10.5194/egusphere-2026-1673
Preprint. Discussion started: 8 April 2026

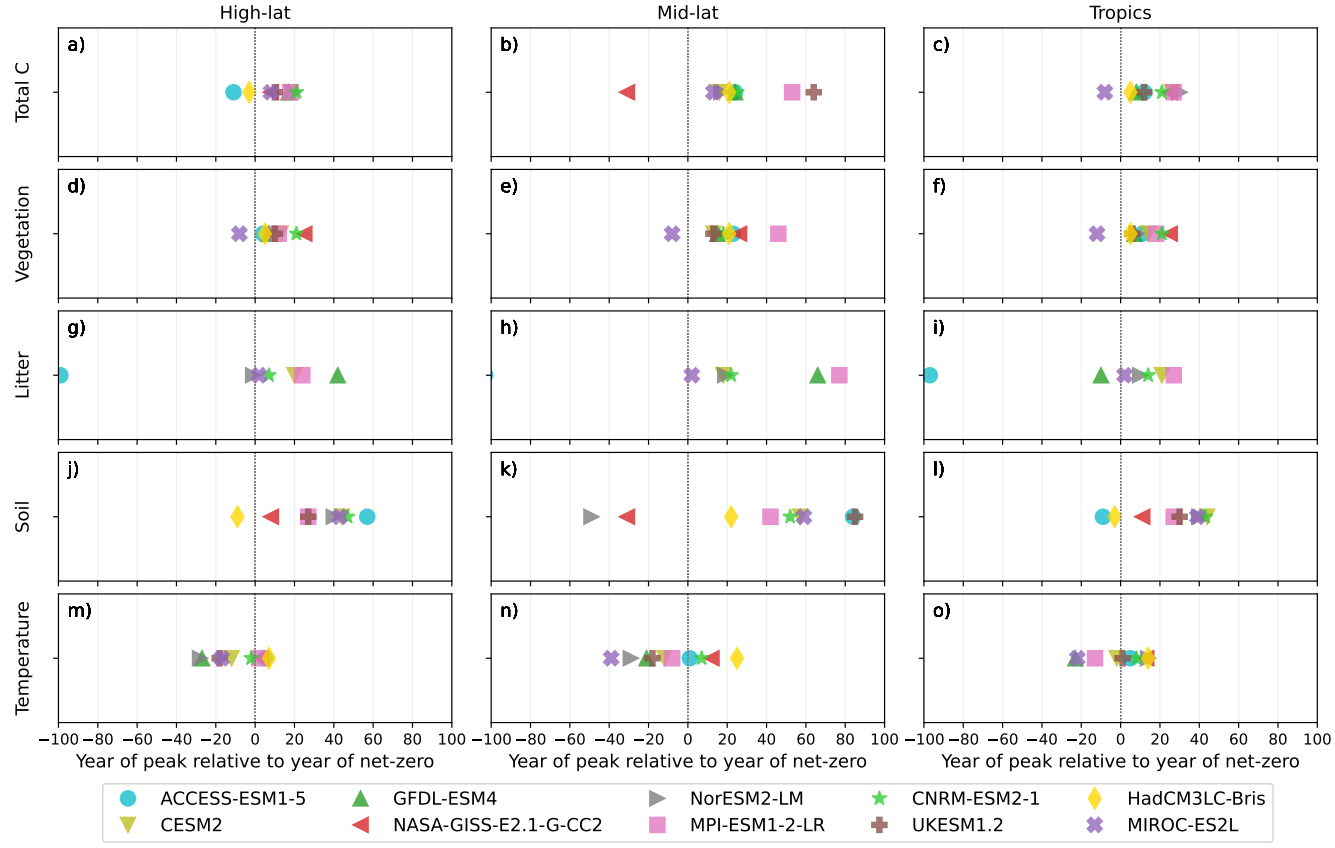

Figure A5. Year of peak relative to year of net-zero for different latitude bands. Each panel shows the year at which that variable reaches its maximum value relative to the year in which emissions reach zero in the esm-flat10-cdr experiment. Each of the ESMs participating in flat10MIP is represented by one symbol. Rows (from top) show total carbon, vegetation carbon, litter carbon, soil carbon, near surface temperature, and globally averaged atmospheric CO_2 concentration. Columns (from left) show global land average, high-latitude land average, mid-latitude land average, and tropical land average.

https://doi.org/10.5194/egusphere-2026-1673
Preprint. Discussion started: 8 April 2026

Table A1. Initial Carbon content and change under different emissions by pool. Carbon stocks and changes in stocks are in units of PgC.

	Initial C Content				Δ Emissions Phase			
ESM	Total C	Vegetation	Litter	Soil	Total C	Vegetation	Litter	Soil
ACCESS-ESM1-5	1516	648	43	825	164	115	6	42
CESM2	1987	554	33	1401	255	202	10	43
GFDL-ESM4	978	438	208	332	252	165	84	3
NASA-GISS-E2.1-G-CC2	1163	291	NaN	872	67	6	NaN	61
NorESM2-LM	3119	540	30	2549	255	206	10	39
MPI-ESM1-2-LR	1390	430	274	685	309	169	64	77
CNRM-ESM2-1	2168	511	214	1443	308	192	50	66
UKESM1.2	2333	592	NaN	1741	237	177	NaN	60
HadCM3LC-Bris	1992	647	NaN	1345	310	164	NaN	145
MIROC-ES2L	1945	526	284	1135	308	155	64	89
Multi-model Mean	1859	518	155	1233	246	155	41	63
Multi-model Standard Dev.	568	98	100	563	71	53	28	34

	Δ Following Net-Zero Emissions				Δ At Cumulative Zero Emissions			
ESM	Total C	Vegetation	Litter	Soil	Total C	Vegetation	Litter	Soil
ACCESS-ESM1-5	4	-4	-2	9	-48	-42	-9	3
CESM2	59	23	-0	37	23	0	-1	24
GFDL-ESM4	52	-4	48	8	31	-35	53	12
NASA-GISS-E2.1-G-CC2	2	4	NaN	-3	5	5	NaN	1
NorESM2-LM	42	11	1	30	-10	-17	-1	7
MPI-ESM1-2-LR	89	24	23	43	26	-18	11	32
CNRM-ESM2-1	33	-10	-7	50	-10	-28	-19	37
UKESM1.2	29	3	NaN	26	13	-10	NaN	23
HadCM3LC-Bris	-23	29	NaN	-52	-31	20	NaN	-51
MIROC-ES2L	10	-36	-11	57	-9	-53	-18	61
Multi-model Mean	30	4	7	21	-1	-18	2	15
Multi-model Standard Dev.	30	18	18	29	23	20	21	27

https://doi.org/10.5194/egusphere-2026-1673
Preprint. Discussion started: 8 April 2026

Table A2. Initial Carbon content and change under different emissions by latitude. Carbon stocks and changes in stocks are in units of PgC.

	Initial C Content				Δ Emissions Phase			
ESM	Total	High-lat	Mid-lat	Tropical	Total	High-lat	Mid-lat	Tropical
ACCESS-ESM1-5	1516	43	3	54	164	70	4	26
CESM2	1987	28	2	70	255	79	4	17
GFDL-ESM4	978	45	21	34	252	65	33	1
NASA-GISS-E2.1-G-CC2	1163	25	NaN	75	67	9	NaN	91
NorESM2-LM	3119	17	1	82	255	81	4	15
MPI-ESM1-2-LR	1390	31	20	49	309	55	21	25
CNRM-ESM2-1	2168	24	10	67	308	62	16	21
UKESM1.2	2333	25	NaN	75	237	75	NaN	25
HadCM3LC-Bris	1992	32	NaN	68	310	53	NaN	47
MIROC-ES2L	1945	27	15	58	308	50	21	29
Multi-model Mean	1859	30	10	63	246	60	15	30
Multi-model Standard Dev.	568	8	7	13	71	19	10	22

	Δ Following Net-Zero Emissions				Δ At Cumulative Zero Emissions			
ESM	Total	High-lat	Mid-lat	Tropical	Total	High-lat	Mid-lat	Tropical
ACCESS-ESM1-5	4	-93	-47	240	-48	88	18	-6
CESM2	59	39	-0	62	23	2	-5	103
GFDL-ESM4	52	-8	92	16	31	-113	174	39
NASA-GISS-E2.1-G-CC2	2	242	NaN	-142	5	87	NaN	13
NorESM2-LM	42	26	2	71	-10	166	8	-74
MPI-ESM1-2-LR	89	27	25	48	26	-69	44	125
CNRM-ESM2-1	33	-32	-21	153	-10	277	182	-359
UKESM1.2	29	11	NaN	89	13	-78	NaN	178
HadCM3LC-Bris	-23	-124	NaN	224	-31	-63	NaN	163
MIROC-ES2L	10	-382	-119	601	-9	582	196	-678
Multi-model Mean	30	-29	-10	136	-1	88	88	-49
Multi-model Standard Dev.	30	143	56	178	23	193	79	244

https://doi.org/10.5194/egusphere-2026-1673
Preprint. Discussion started: 8 April 2026

Table A3. Lead or lag of peak relative to year of net-zero emissions for each latitude band. Each column represents the lead or lag for a given variable in years.

	Global						High-latitude				
ESM	Tot. C	Veg.	Litter	Soil	Temp.	CO_2	Tot. C	Veg.	Litter	Soil	Temp.
ACCESS-ESM1-5	-11	4	-99	57	5	-10	24	23	-103	84	1
CESM2	18	13	20	44	-12	-22	16	13	18	57	-12
GFDL-ESM4	17	7	42	126	-27	-18	24	15	66	146	-21
NASA-GISS-E2.1-G-CC2	8	25	NaN	8	3	-16	-31	26	NaN	-31	12
NorESM2-LM	19	9	-1	40	-28	-22	17	16	19	-49	-29
MPI-ESM1-2-LR	18	12	24	27	2	-26	53	46	77	42	-8
CNRM-ESM2-1	21	21	7	47	-2	-23	25	18	22	52	7
UKESM1.2	10	10	NaN	27	-18	-10	64	13	NaN	85	-18
HadCM3LC-Bris	-3	5	NaN	-9	7	-16	21	21	NaN	22	25
MIROC-ES2L	8	-8	2	43	-17	-23	13	-8	2	59	-39
Multi-model Mean	9	10	2	35	-4	-14	20	17	19	40	-3
Multi-model Standard Dev.	10	8	40	32	18	10	22	12	48	50	22

	Mid-Latitude					Tropical				
ESM	Tot. C	Veg.	Litter	Soil	Temp.	Tot. C	Veg.	Litter	Soil	Temp.
ACCESS-ESM1-5	12	11	-97	-9	5	-40	-37	-99	-75	15
CESM2	26	14	21	44	-2	13	13	20	35	-2
GFDL-ESM4	8	7	-10	116	-23	-10	7	-9	-84	5
NASA-GISS-E2.1-G-CC2	25	25	NaN	11	13	2	12	NaN	-9	4
NorESM2-LM	30	8	10	40	14	13	13	14	39	-11
MPI-ESM1-2-LR	27	18	27	27	-13	13	6	20	24	14
CNRM-ESM2-1	21	21	14	43	8	-18	-18	-67	-61	-8
UKESM1.2	12	6	NaN	30	1	-20	-20	NaN	-50	-14
HadCM3LC-Bris	5	5	NaN	-3	14	-15	-9	NaN	-42	11
MIROC-ES2L	-8	-12	2	39	-22	3	-8	-5	8	-17
Multi-model Mean	17	12	6	31	5	-3	-1	-7	-16	4
Multi-model Standard Dev.	11	10	39	31	18	16	15	41	41	15

https://doi.org/10.5194/egusphere-2026-1673
Preprint. Discussion started: 8 April 2026

Author contributions. ALSS conceptualized, completed the analysis, and wrote the initial draft. CDK, CP, RAF, and BS contributed to conceptualization. VB, TH, CDJ, NYK, DML, SL, HL, AR, RF, LTS, NJS, JT, and TZ contributed model simulations for analysis. All authors reviewed and edited the manuscript.

Competing interests. The authors declare no competing interests.

Acknowledgements. ALSS acknowledges support from the US National Science Foundation (grant no. AGS-2330096). This material is based upon work supported by the National Center for Atmospheric Research (NCAR), which is a major facility sponsored by the US National Science Foundation under Cooperative Agreement No. 1852977. We acknowledge computing support and data storage resources provided by NCAR's Computational and Information Systems Laboratory, sponsored by the National Science Foundation. NYK, HL, and AR were supported by the NASA Modeling, Analysis, and Prediction (MAP) program. Resources supporting their work were provided by the NASA High-End Computing (HEC) Program through the NASA Center for Climate Simulation (NCCS) at Goddard Space Flight Center. CDJ and SKL were supported by the Met Office Hadley Centre Climate Programme funded by DSIT. VB acknowledges funding by the European Research Council under the European Union's Horizon 2020 Research and Innovation programme as part of the Q-Arctic project (grant agreement number 951288). TZ received funding from the Australian Government under the National Environmental Science Program. ACCESS-ESM1-5 simulations were undertaken with the assistance of resources from the National Computational Infrastructure (NCI Australia), an NCRIS enabled capability supported by the Australian Government. The MPI-ESM1-2-LR simulations used resources of the Deutsches Klimarechenzentrum (DKRZ) granted by its Scientific Steering Committee (WLA) under project ID bm1124. TH is supported by the MEXT-Program for the Advanced Studies of Climate Change Projection (SENTAN, grant no. JPMXD0722681344) and by the Environment Research and Technology Development Fund (grant no. JPMEERF24S12204) of the Environmental Restoration and Conservation Agency of the Ministry of Environment of Japan. CNRM-ESM simulations used resources from the Météo-France/DSI supercomputing center and support from the French national Research Infrastructure CLIMERI-France (https://climeri-france.fr/). R.S., received support from the European Union's Horizon 2020 research and innovation programme under Grant Agreement N° 101003536 (ESM2025) and N° 101081193 (OptimESM). John Dunne (NOAA/GFDL) is acknowledged for feedback on the manuscript's internal review.

https://doi.org/10.5194/egusphere-2026-1673
Preprint. Discussion started: 8 April 2026

References

Adcroft, A., Anderson, W., Balaji, V., Blanton, C., Bushuk, M., Dufour, C. O., Dunne, J. P., Griffies, S. M., Hallberg, R., Harrison, M. J., Held, I. M., Jansen, M. F., John, J. G., Krasting, J. P., Langenhorst, A. R., Legg, S., Liang, Z., McHugh, C., Radhakrishnan, A., Reichl, B. G., Rosati, T., Samuels, B. L., Shao, A., Stouffer, R., Winton, M., Wittenberg, A. T., Xiang, B., Zadeh, N., and Zhang, R.: The GFDL Global Ocean and Sea Ice Model OM4.0: Model Description and Simulation Features, Journal of Advances in Modeling Earth Systems, 11, 3167–3211, https://doi.org/https://doi.org/10.1029/2019MS001726, 2019.

Allen, C. D., Breshears, D. D., and McDowell, N. G.: On underestimation of global vulnerability to tree mortality and forest die-off from hotter drought in the Anthropocene, Ecosphere, 6, art129, https://doi.org/10.1890/ES15-00203.1, 2015.

Allen, M. R., Frame, D. J., Huntingford, C., Jones, C. D., Lowe, J. A., Meinshausen, M., and Meinshausen, N.: Warming caused by cumulative carbon emissions towards the trillionth tonne, Nature, 458, 1163–1166, https://doi.org/10.1038/nature08019, 2009.

Arora, V. K., Katavouta, A., Williams, R. G., Jones, C. D., Brovkin, V., Friedlingstein, P., Schwinger, J., Bopp, L., Boucher, O., Cadule, P., Chamberlain, M. A., Christian, J. R., Delire, C., Fisher, R. A., Hajima, T., Ilyina, T., Joetzjer, E., Kawamiya, M., Koven, C. D., Krasting, J. P., Law, R. M., Lawrence, D. M., Lenton, A., Lindsay, K., Pongratz, J., Raddatz, T., Séférian, R., Tachiiri, K., Tjiputra, J. F., Wiltshire, A., Wu, T., and Ziehn, T.: Carbon–concentration and carbon–climate feedbacks in CMIP6 models and their comparison to CMIP5 models, Biogeosciences, 17, 4173–4222, https://doi.org/10.5194/bg-17-4173-2020, 2020.

Asaadi, A., Schwinger, J., Lee, H., Tjiputra, J., Arora, V., Séférian, R., Liddicoat, S., Hajima, T., Santana-Falcón, Y., and Jones, C. D.: Carbon cycle feedbacks in an idealized simulation and a scenario simulation of negative emissions in CMIP6 Earth system models, Biogeosciences, 21, 411–435, https://doi.org/10.5194/bg-21-411-2024, 2024.

Atkin, O. K. and Tjoelker, M. G.: Thermal acclimation and the dynamic response of plant respiration to temperature, Trends in Plant Science, 8, 343–351, https://doi.org/10.1016/S1360-1385(03)00136-5, 2003.

Ball, J. T., Woodrow, I. E., and Berry, J. A.: A Model Predicting Stomatal Conductance and its Contribution to the Control of Photosynthesis under Different Environmental Conditions, pp. 221–224, Springer Netherlands, Dordrecht, https://doi.org/10.1007/978-94-017-0519-6_48, 1987.

Bar-On, Y. M., Li, X., O'Sullivan, M., Wigneron, J.-P., Sitch, S., Ciais, P., Frankenberg, C., and Fischer, W. W.: Recent gains in global terrestrial carbon stocks are mostly stored in nonliving pools, Science, 387, 1291–1295, https://doi.org/10.1126/science.adk1637, 2025.

Batjes, N. H.: Harmonized soil property values for broad-scale modelling (WISE30sec) with estimates of global soil carbon stocks, Geoderma, 269, 61–68, https://doi.org/https://doi.org/10.1016/j.geoderma.2016.01.034, 2016.

Bennett, A. C., McDowell, N. G., Allen, C. D., and Anderson-Teixeira, K. J.: Larger trees suffer most during drought in forests worldwide, Nature Plants, 1, 15 139, https://doi.org/10.1038/nplants.2015.139, 2015.

Bita, C. and Gerats, T.: Plant tolerance to high temperature in a changing environment: scientific fundamentals and production of heat stress-tolerant crops, Frontiers in Plant Science, Volume 4 - 2013, https://doi.org/10.3389/fpls.2013.00273, 2013.

Bonan, G.: Ecological climatology: concepts and applications, Cambridge University Press, 2015.

Booth, B., Jones, C., Collins, M., Totterdell, I., Cox, P., Sitch, S., Huntingford, C., Betts, R., Harris, G., and Lloyd, J.: High sensitivity of future global warming to land carbon cycle processes, Environmental Research Letters, 7, 024 002, https://doi.org/10.1088/1748-9326/7/2/024002, 2012.

https://doi.org/10.5194/egusphere-2026-1673
Preprint. Discussion started: 8 April 2026

Bossert, I., Baur, S., Cussac, M., Berthet, S., Delire, C., Michou, M., Nabat, P., Roehrig, R., Voldoire, A., and Séférian, R.: CNRM-ESM2-2: development and evaluation of an updated version of the CNRM-CERFACS Earth System Model, https://doi.org/10.22541/essoar.175977424.42948487/v1, 2025.

Brovkin, V., Raddatz, T., Reick, C. H., Claussen, M., and Gayler, V.: Global biogeophysical interactions between forest and climate, Geophysical Research Letters, 36, https://doi.org/ARTN L07405, 2009.

Brovkin, V., Sanderson, B. M., Brizuela, N. G., Hajima, T., Ilyina, T., Jones, C. D., Koven, C., Lawrence, D., Lawrence, P., Li, H., Liddcoat, S., Romanou, A., Séférian, R., Sentman, L. T., Swann, A. L. S., Tjiputra, J., Ziehn, T., and Winkler, A. J.: On a simplified solution of climate-carbon dynamics in idealized flat10MIP simulations, Earth System Dynamics, 16, 2021–2034, https://doi.org/10.5194/esd-16-2021-2025, 2025.

Canadell, J., Monteiro, P., Costa, M., Cotrim da Cunha, L., Cox, P., Eliseev, A., Henson, S., Ishii, M., Jaccard, S., Koven, C., Lohila, A., Patra, P., Piao, S., Rogelj, J., Syampungani, S., Zaehle, S., and Zickfeld, K.: Global Carbon and other Biogeochemical Cycles and Feedbacks, pp. 673–816, Cambridge University Press, Cambridge, United Kingdom and New York, NY, USA, https://doi.org/10.1017/9781009157896.007, 2021.

Clark, D. B., Mercado, L. M., Sitch, S., Jones, C. D., Gedney, N., Best, M. J., Pryor, M., Rooney, G. G., Essery, R. L. H., Blyth, E., Boucher, O., Harding, R. J., Huntingford, C., and Cox, P. M.: The Joint UK Land Environment Simulator (JULES), model description â Part 2: Carbon fluxes and vegetation dynamics, Geoscientific Model Development, 4, 701–722, https://doi.org/10.5194/gmd-4-701-2011, 2011.

Collatz, G. J., Ball, J. T., Grivet, C., and Berry, J. A.: Physiological and Environmental-Regulation of Stomatal Conductance, Photosynthesis and Transpiration - a Model That Includes a Laminar Boundary-Layer, Agricultural and Forest Meteorology, 54, 107–136, 1991.

Collatz, G. J., Berry, J., and Clark, J. S.: Effects of climate and atmospheric CO2 partial pressure on the global distribution of C4 grasses: present, past, and future, Oecologia, 114, 441–454, 1998.

Cook-Patton, S. C., Leavitt, S. M., Gibbs, D., Harris, N. L., Lister, K., Anderson-Teixeira, K. J., Briggs, R. D., Chazdon, R. L., Crowther, T. W., Ellis, P. W., Griscom, H. P., Herrmann, V., Holl, K. D., Houghton, R. A., Larrosa, C., Lomax, G., Lucas, R., Madsen, P., Malhi, Y., Paquette, A., Parker, J. D., Paul, K., Routh, D., Roxburgh, S., Saatchi, S., van den Hoogen, J., Walker, W. S., Wheeler, C. E., Wood, S. A., Xu, L., and Griscom, B. W.: Mapping carbon accumulation potential from global natural forest regrowth, Nature, 585, 545–550, https://doi.org/10.1038/s41586-020-2686-x, 2020.

Cox, P. M.: Description of the TRIFFID dynamic global vegetation model, Tech. rep., Technical Note 24, Hadley Centre, United Kingdom Meteorological Office, Bracknell, UK, 2001.

Cramer, W., Bondeau, A., Woodward, F. I., Prentice, I. C., Betts, R. A., Brovkin, V., Cox, P. M., Fisher, V., Foley, J. A., Friend, A. D., Kucharik, C., Lomas, M. R., Ramankutty, N., Sitch, S., Smith, B., White, A., and Young-Molling, C.: Global response of terrestrial ecosystem structure and function to CO2 and climate change: results from six dynamic global vegetation models, Global Change Biology, 7, 357–373, https://doi.org/10.1046/j.1365-2486.2001.00383.x, 2001.

Danabasoglu, G., Lamarque, J.-F., Bacmeister, J., Bailey, D. A., DuVivier, A. K., Edwards, J., Emmons, L. K., Fasullo, J., Garcia, R., Gettelman, A., Hannay, C., Holland, M. M., Large, W. G., Lauritzen, P. H., Lawrence, D. M., Lenaerts, J. T. M., Lindsay, K., Lipscomb, W. H., Mills, M. J., Neale, R., Oleson, K. W., Otto-Bliesner, B., Phillips, A. S., Sacks, W., Tilmes, S., van Kampenhout, L., Vertenstein, M., Bertini, A., Dennis, J., Deser, C., Fischer, C., Fox-Kemper, B., Kay, J. E., Kinnison, D., Kushner, P. J., Larson, V. E., Long, M. C., Mickelson, S., Moore, J. K., Nienhouse, E., Polvani, L., Rasch, P. J., and Strand, W. G.: The Community Earth System Model Version 2 (CESM2), Journal of Advances in Modeling Earth Systems, 12, e2019MS001 916, https://doi.org/10.1029/2019MS001916, _eprint: https://onlinelibrary.wiley.com/doi/pdf/10.1029/2019MS001916, 2020.

https://doi.org/10.5194/egusphere-2026-1673
Preprint. Discussion started: 8 April 2026

Decharme, B. and Colin, J.: Influence of floodplains and groundwater dynamics on the present-day climate simulated by the CNRM climate model, Earth System Dynamics, 16, 729–752, https://doi.org/10.5194/esd-16-729-2025, 2025.

Decharme, B., Delire, C., Minvielle, M., Colin, J., Vergnes, J.-P., Alias, A., Saint-Martin, D., Séférian, R., Sénési, S., and Voldoire, A.: Recent Changes in the ISBA-CTRIP Land Surface System for Use in the CNRM-CM6 Climate Model and in Global Off-Line Hydrological Applications, Journal of Advances in Modeling Earth Systems, 11, 1207–1252, https://doi.org/https://doi.org/10.1029/2018MS001545, 2019.

Delire, C., Séférian, R., Decharme, B., Alkama, R., Calvet, J.-C., Carrer, D., Gibelin, A.-L., Joetzjer, E., Morel, X., Rocher, M., and Tzanos, D.: The Global Land Carbon Cycle Simulated With ISBA-CTRIP: Improvements Over the Last Decade, Journal of Advances in Modeling Earth Systems, 12, e2019MS001 886, https://doi.org/https://doi.org/10.1029/2019MS001886, 2020.

Doney, S. C., Lindsay, K., Fung, I., and John, J.: Natural variability in a stable, 1000-yr global coupled climate-carbon cycle simulation, Journal of Climate, 19, 3033–3054, 063NO Times Cited:1 Cited References Count:59, 2006.

Dunne, J. P., Horowitz, L. W., Adcroft, A. J., Ginoux, P., Held, I. M., John, J. G., Krasting, J. P., Malyshev, S., Naik, V., Paulot, F., Shevliakova, E., Stock, C. A., Zadeh, N., Balaji, V., Blanton, C., Dunne, K. A., Dupuis, C., Durachta, J., Dussin, R., Gauthier, P. P. G., Griffies, S. M., Guo, H., Hallberg, R. W., Harrison, M., He, J., Hurlin, W., McHugh, C., Menzel, R., Milly, P. C. D., Nikonov, S., Paynter, D. J., Ploshay, J., Radhakrishnan, A., Rand, K., Reichl, B. G., Robinson, T., Schwarzkopf, D. M., Sentman, L. T., Underwood, S., Vahlenkamp, H., Winton, M., Wittenberg, A. T., Wyman, B., Zeng, Y., and Zhao, M.: The GFDL Earth System Model Version 4.1 (GFDL-ESM 4.1): Overall Coupled Model Description and Simulation Characteristics, Journal of Advances in Modeling Earth Systems, 12, e2019MS002 015, https://doi.org/https://doi.org/10.1029/2019MS002015, 2020.

Essery, R. L. H., Best, M. J., Betts, R. A., Cox, P. M., and Taylor, C. M.: Explicit Representation of Subgrid Heterogeneity in a GCM Land Surface Scheme, Journal of Hydrometeorology, 4, 530 – 543, https://doi.org/10.1175/1525-7541(2003)004<0530:EROSHI>2.0.CO;2, 2003.

Evans, S., Ginoux, P., Malyshev, S., and Shevliakova, E.: Climate-vegetation interaction and amplification of Australian dust variability, Geophysical Research Letters, 43, 11,823–11,830, https://doi.org/https://doi.org/10.1002/2016GL071016, 2016.

Evans, S., Malyshev, S., Ginoux, P., and Shevliakova, E.: The Impacts of the Dust Radiative Effect on Vegetation Growth in the Sahel, Global Biogeochemical Cycles, 33, 1582–1593, https://doi.org/https://doi.org/10.1029/2018GB006128, 2019.

Eyring, V., Bony, S., Meehl, G. A., Senior, C. A., Stevens, B., Stouffer, R. J., and Taylor, K. E.: Overview of the Coupled Model Intercomparison Project Phase 6 (CMIP6) experimental design and organization, Geoscientific Model Development, 9, 1937–1958, https://doi.org/10.5194/gmd-9-1937-2016, 2016.

Fao, I.: Harmonized world soil database version 2.0. Rome and Laxenburg, 2023.

Farquhar, G. and Von Caemmerer, S.: Modelling of photosynthetic response to environmental conditions, in: Physiological Plant Ecology II, pp. 549–587, Springer, 1982.

Farquhar, G., von Caemmerer, S., and Berry, J.: A Biochemical-Model of Photosynthetic CO2 Assimilation in Leaves of C-3 Species, Planta, 149, 78–90, 1980.

Ficklin, D. L. and Novick, K. A.: Historic and projected changes in vapor pressure deficit suggest a continental-scale drying of the United States atmosphere, Journal of Geophysical Research: Atmospheres, 122, 2061–2079, https://doi.org/https://doi.org/10.1002/2016JD025855, 2017.

https://doi.org/10.5194/egusphere-2026-1673
Preprint. Discussion started: 8 April 2026

Fisher, R. A., Wieder, W. R., Sanderson, B. M., Koven, C. D., Oleson, K. W., Xu, C., Fisher, J. B., Shi, M., Walker, A. P., and Lawrence, D. M.: Parametric controls on vegetation responses to biogeochemical forcing in the CLM5, Journal of Advances in Modeling Earth Systems, 11, 2879–2895, 2019.

Friedlingstein, P., Cox, P., Betts, R., Bopp, L., Von Bloh, W., Brovkin, V., Cadule, P., Doney, S., Eby, M., Fung, I., Bala, G., John, J., Jones, C., Joos, F., Kato, T., Kawamiya, M., Knorr, W., Lindsay, K., Matthews, H. D., Raddatz, T., Rayner, P., Reick, C., Roeckner, E., Schnitzler, K. G., Schnur, R., Strassmann, K., Weaver, A. J., Yoshikawa, C., and Zeng, N.: Climate-carbon cycle feedback analysis: results from the C4MIP model intercomparison, Journal of Climate, 19, 3337–3353, https://doi.org/10.1175/JCLI3800.1, 063NP Times Cited:1 Cited References Count:111, 2006.

Friedlingstein, P., Meinshausen, M., Arora, V. K., Jones, C. D., Anav, A., Liddicoat, S. K., and Knutti, R.: Uncertainties in CMIP5 Climate Projections due to Carbon Cycle Feedbacks, Journal of Climate, 27, 511–526, https://doi.org/10.1175/JCLI-D-12-00579.1, 2014.

Friedlingstein, P., O'Sullivan, M., Jones, M. W., Andrew, R. M., Hauck, J., Landschützer, P., Le Quéré, C., Li, H., Luijkx, I. T., Olsen, A., Peters, G. P., Peters, W., Pongratz, J., Schwingshackl, C., Sitch, S., Canadell, J. G., Ciais, P., Jackson, R. B., Alin, S. R., Arneth, A., Arora, V., Bates, N. R., Becker, M., Bellouin, N., Berghoff, C. F., Bittig, H. C., Bopp, L., Cadule, P., Campbell, K., Chamberlain, M. A., Chandra, N., Chevallier, F., Chini, L. P., Colligan, T., Decayeux, J., Djeutchouang, L., Dou, X., Duran Rojas, C., Enyo, K., Evans, W., Fay, A., Feely, R. A., Ford, D. J., Foster, A., Gasser, T., Gehlen, M., Gkritzalis, T., Grassi, G., Gregor, L., Gruber, N., Gürses, O., Harris, I., Hefner, M., Heinke, J., Hurtt, G. C., Iida, Y., Ilyina, T., Jacobson, A. R., Jain, A., Jarníková, T., Jersild, A., Jiang, F., Jin, Z., Kato, E., Keeling, R. F., Klein Goldewijk, K., Knauer, J., Korsbakken, J. I., Lauvset, S. K., Lefèvre, N., Liu, Z., Liu, J., Ma, L., Maksyutov, S., Marland, G., Mayot, N., McGuire, P., Metzl, N., Monacci, N. M., Morgan, E. J., Nakaoka, S.-I., Neill, C., Niwa, Y., Nützel, T., Olivier, L., Ono, T., Palmer, P. I., Pierrot, D., Qin, Z., Resplandy, L., Roobaert, A., Rosan, T. M., Rödenbeck, C., Schwinger, J., Smallman, T. L., Smith, S., Sospedra-Alfonso, R., Steinhoff, T., Sun, Q., Sutton, A. J., Séférian, R., Takao, S., Tatebe, H., Tian, H., Tilbrook, B., Torres, O., Tourigny, E., Tsujino, H., Tubiello, F., van der Werf, G., Wanninkhof, R., Wang, X., Yang, D., Yang, X., Yu, Z., Yuan, W., Yue, X., Zaehle, S., Zeng, N., and Zeng, J.: Global Carbon Budget 2024, Earth System Science Data Discussions, 2024, 1–133, https://doi.org/10.5194/essd-2024-519, 2024.

Friedlingstein, P., O'Sullivan, M., Jones, M. W., Andrew, R. M., Bakker, D. C. E., Hauck, J., Landschützer, P., Le Quéré, C., Li, H., Luijkx, I. T., Peters, G. P., Peters, W., Pongratz, J., Schwingshackl, C., Sitch, S., Canadell, J. G., Ciais, P., Aas, K., Alin, S. R., Anthoni, P., Barbero, L., Bates, N. R., Bellouin, N., Benoit-Cattin, A., Berghoff, C. F., Bernardello, R., Bopp, L., Brasika, I. B. M., Chamberlain, M. A., Chandra, N., Chevallier, F., Chini, L. P., Collier, N. O., Colligan, T. H., Cronin, M., Djeutchouang, L., Dou, X., Enright, M. P., Enyo, K., Erb, M., Evans, W., Feely, R. A., Feng, L., Ford, D. J., Foster, A., Fransner, F., Gasser, T., Gehlen, M., Gkritzalis, T., Goncalves De Souza, J., Grassi, G., Gregor, L., Gruber, N., Guenet, B., Gürses, O., Harrington, K., Harris, I., Heinke, J., Hurtt, G. C., Iida, Y., Ilyina, T., Ito, A., Jacobson, A. R., Jain, A. K., Jarníková, T., Jersild, A., Jiang, F., Jones, S. D., Kato, E., Keeling, R. F., Klein Goldewijk, K., Knauer, J., Kong, Y., Korsbakken, J. I., Koven, C., Kunimitsu, T., Lan, X., Liu, J., Liu, Z., Liu, Z., Lo Monaco, C., Ma, L., Marland, G., McGuire, P. C., McKinley, G. A., Melton, J., Monacci, N., Monier, E., Morgan, E. J., Munro, D. R., Müller, J. D., Nakaoka, S.-I., Nayagam, L. R., Niwa, Y., Nutzel, T., Olsen, A., Omar, A. M., Pan, N., Pandey, S., Pierrot, D., Qin, Z., Regnier, P. A. G., Rehder, G., Resplandy, L., Roobaert, A., Rosan, T. M., Rödenbeck, C., Schwinger, J., Skjelvan, I., Smallman, T. L., Spada, V., Sreeush, M. G., Sun, Q., Sutton, A. J., Sweeney, C., Swingedouw, D., Séférian, R., Takao, S., Tatebe, H., Tian, H., Tian, X., Tilbrook, B., Tsujino, H., Tubiello, F., van Ooijen, E., van der Werf, G., van de Velde, S. J., Walker, A., Wanninkhof, R., Yang, X., Yuan, W., Yue, X., and Zeng, J.: Global Carbon Budget 2025, Earth System Science Data Discussions, 2025, 1–139, https://doi.org/10.5194/essd-2025-659, 2025.

https://doi.org/10.5194/egusphere-2026-1673
Preprint. Discussion started: 8 April 2026

Gazol, A. and Camarero, J. J.: Compound climate events increase tree drought mortality across European forests, Science of The Total Environment, 816, 151 604, https://doi.org/https://doi.org/10.1016/j.scitotenv.2021.151604, 2022.

Gazol, A., Pizarro, M., Hammond, W. M., Allen, C. D., and Camarero, J. J.: Droughts preceding tree mortality events have increased in duration and intensity, especially in dry biomes, Nature Communications, 16, 5779, https://doi.org/10.1038/s41467-025-60856-5, 2025.

Goll, D. S., Winkler, A. J., Raddatz, T., Dong, N., Prentice, I. C., Ciais, P., and Brovkin, V.: Carbon–nitrogen interactions in idealized simulations with JSBACH (version 3.10), Geoscientific Model Development, 10, 2009–2030, https://doi.org/10.5194/gmd-10-2009-2017, 2017.

Gordon, C., Cooper, C., Senior, C. A., Banks, H., Gregory, J. M., Johns, T. C., Mitchell, J. F. B., and Wood, R. A.: The simulation of SST, sea ice extents and ocean heat transports in a version of the Hadley Centre coupled model without flux adjustments, Climate Dynamics, 16, 147–168, https://doi.org/10.1007/s003820050010, 2000.

Griscom, B. W., Adams, J., Ellis, P. W., Houghton, R. A., Lomax, G., Miteva, D. A., Schlesinger, W. H., Shoch, D., Siikamäki, J. V., Smith, P., Woodbury, P., Zganjar, C., Blackman, A., Campari, J., Conant, R. T., Delgado, C., Elias, P., Gopalakrishna, T., Hamsik, M. R., Herrero, M., Kiesecker, J., Landis, E., Laestadius, L., Leavitt, S. M., Minnemeyer, S., Polasky, S., Potapov, P., Putz, F. E., Sanderman, J., Silvius, M., Wollenberg, E., and Fargione, J.: Natural climate solutions, Proceedings of the National Academy of Sciences, 114, 11 645–11 650, https://doi.org/10.1073/pnas.1710465114, 2017.

Grossiord, C., Buckley, T. N., Cernusak, L. A., Novick, K. A., Poulter, B., Siegwolf, R. T. W., Sperry, J. S., and McDowell, N. G.: Plant responses to rising vapor pressure deficit, New Phytologist, 226, 1550–1566, https://doi.org/https://doi.org/10.1111/nph.16485, 2020.

Haberstroh, S., Werner, C., Grün, M., Kreuzwieser, J., Seifert, T., Schindler, D., and Christen, A.: Central European 2018 hot drought shifts scots pine forest to its tipping point, Plant Biology, 24, 1186–1197, https://doi.org/https://doi.org/10.1111/plb.13455, 2022.

Hajima, T., Watanabe, M., Yamamoto, A., Tatebe, H., Noguchi, M. A., Abe, M., Ohgaito, R., Ito, A., Yamazaki, D., Okajima, H., Ito, A., Takata, K., Ogochi, K., Watanabe, S., and Kawamiya, M.: Development of the MIROC-ES2L Earth system model and the evaluation of biogeochemical processes and feedbacks, Geoscientific Model Development, 13, 2197–2244, https://doi.org/10.5194/gmd-13-2197-2020, 2020.

Hajima, T., Kawamiya, M., Ito, A., Tachiiri, K., Jones, C. D., Arora, V., Brovkin, V., Séférian, R., Liddicoat, S., Friedlingstein, P., and Shevliakova, E.: Consistency of global carbon budget between concentration- and emission-driven historical experiments simulated by CMIP6 Earth system models and suggestions for improved simulation of CO_2 concentration, Biogeosciences, 22, 1447–1473, https://doi.org/10.5194/bg-22-1447-2025, 2025.

Harper, A. B., Cox, P. M., Friedlingstein, P., Wiltshire, A. J., Jones, C. D., Sitch, S., Mercado, L. M., Groenendijk, M., Robertson, E., Kattge, J., Bönisch, G., Atkin, O. K., Bahn, M., Cornelissen, J., Niinemets, U., Onipchenko, V., Peñuelas, J., Poorter, L., Reich, P. B., Soudzilovskaia, N. A., and Bodegom, P. V.: Improved representation of plant functional types and physiology in the Joint UK Land Environment Simulator (JULES v4.2) using plant trait information, Geoscientific Model Development, 9, 2415–2440, https://doi.org/10.5194/gmd-9-2415-2016, 2016.

Hartmann, H., Bastos, A., Das, A. J., Esquivel-Muelbert, A., Hammond, W. M., MartÃ-nez Vilalta, J., McDowell, N. G., Powers, J. S., Pugh, T. A., Ruthrof, K. X., and Allen, C. D.: Climate Change Risks to Global Forest Health: Emergence of Unexpected Events of Elevated Tree Mortality Worldwide, Annual Review of Plant Biology, 73, 673–702, https://doi.org/https://doi.org/10.1146/annurev-arplant-102820-012804, 2022.

Horowitz, L. W., Naik, V., Paulot, F., Ginoux, P. A., Dunne, J. P., Mao, J., Schnell, J., Chen, X., He, J., John, J. G., Lin, M., Lin, P., Malyshev, S., Paynter, D., Shevliakova, E., and Zhao, M.: The GFDL Global Atmospheric Chemistry-Climate Model

https://doi.org/10.5194/egusphere-2026-1673
Preprint. Discussion started: 8 April 2026

AM4.1: Model Description and Simulation Characteristics, Journal of Advances in Modeling Earth Systems, 12, e2019MS002 032, https://doi.org/10.1029/2019MS002032, _eprint: https://onlinelibrary.wiley.com/doi/pdf/10.1029/2019MS002032, 2020.

Hugelius, G., Strauss, J., Zubrzycki, S., Harden, J. W., Schuur, E. A. G., Ping, C.-L., Schirrmeister, L., Grosse, G., Michaelson, G. J., Koven, C. D., O'Donnell, J. A., Elberling, B., Mishra, U., Camill, P., Yu, Z., Palmtag, J., and Kuhry, P.: Estimated stocks of circumpolar permafrost carbon with quantified uncertainty ranges and identified data gaps, Biogeosciences, 11, 6573–6593, https://doi.org/10.5194/bg-11-6573-2014, 2014.

Hurtt, G. C., Chini, L., Sahajpal, R., Frolking, S., Bodirsky, B. L., Calvin, K., Doelman, J. C., Fisk, J., Fujimori, S., Klein Goldewijk, K., Hasegawa, T., Havlik, P., Heinimann, A., Humpenöder, F., Jungclaus, J., Kaplan, J. O., Kennedy, J., Krisztin, T., Lawrence, D., Lawrence, P., Ma, L., Mertz, O., Pongratz, J., Popp, A., Poulter, B., Riahi, K., Shevliakova, E., Stehfest, E., Thornton, P., Tubiello, F. N., van Vuuren, D. P., and Zhang, X.: Harmonization of global land use change and management for the period 850–2100 (LUH2) for CMIP6, Geoscientific Model Development, 13, 5425–5464, https://doi.org/10.5194/gmd-13-5425-2020, 2020.

Ito, A. and Inatomi, M.: Water-Use Efficiency of the Terrestrial Biosphere: A Model Analysis Focusing on Interactions between the Global Carbon and Water Cycles, Journal of Hydrometeorology, 13, 681–694, https://doi.org/https://doi.org/10.1175/JHM-D-10-05034.1, 2012.

Ito, A., Hajima, T., Lawrence, D. M., Brovkin, V., Delire, C., Guenet, B., Jones, C. D., Malyshev, S., Materia, S., McDermid, S. P., Peano, D., Pongratz, J., Robertson, E., Shevliakova, E., Vuichard, N., WÃ¥rlind, D., Wiltshire, A., and Ziehn, T.: Soil carbon sequestration simulated in CMIP6-LUMIP models: implications for climatic mitigation, Environmental Research Letters, 15, 124 061, https://doi.org/10.1088/1748-9326/abc912, 2020a.

Ito, G., Romanou, A., Kiang, N. Y., Faluvegi, G., Aleinov, I., Ruedy, R., Russell, G., Lerner, P., Kelley, M., and Lo, K.: Global Carbon Cycle and Climate Feedbacks in the NASA GISS ModelE2.1, Journal of Advances in Modeling Earth Systems, 12, e2019MS002 030, https://doi.org/https://doi.org/10.1029/2019MS002030, 2020b.

Jackson, R. B., Lajtha, K., Crow, S. E., Hugelius, G., Kramer, M. G., and PiÃ±eiro, G.: The Ecology of Soil Carbon: Pools, Vulnerabilities, and Biotic and Abiotic Controls, Annual Review of Ecology, Evolution, and Systematics, 48, 419–445, https://doi.org/https://doi.org/10.1146/annurev-ecolsys-112414-054234, 2017.

Jagadish, S. V. K., Way, D. A., and Sharkey, T. D.: Plant heat stress: Concepts directing future research, Plant, Cell & Environment, 44, 1992–2005, https://doi.org/https://doi.org/10.1111/pce.14050, 2021.

Jeevanjee, N., Paynter, D. J., Dunne, J. P., Sentman, L. T., and Krasting, J. P.: A Holistic View of Climate Sensitivity, Annual Review of Earth and Planetary Sciences, 53, 367–396, https://doi.org/https://doi.org/10.1146/annurev-earth-040523-014302, 2025.

Jones, C., McConnell, C., Coleman, K., Cox, P., Falloon, P., Jenkinson, D., and Powlson, D.: Global climate change and soil carbon stocks; predictions from two contrasting models for the turnover of organic carbon in soil, Global Change Biology, 11, 154–166, times Cited: 4, 2005.

Jones, C., Bossert, I., Dennis, D. P., Jeffery, H., Jones, C. D., Koenigk, T., Loriani, S., Sanderson, B., Séférian, R., Wyser, K., Yang, S., Abe, M., Bathiany, S., Braconnot, P., Brovkin, V., Burger, F. A., Cadule, P., Castruccio, F. S., Danabasoglu, G., Dittus, A., Donges, J. F., Fröb, F., Frölicher, T., Georgievski, G., Guo, C., Hu, A., Lawrence, P., Lerner, P., Licón-Saláiz, J., Otto-Bliesner, B., Romanou, A., Shevliakova, E., Silvy, Y., Swingedouw, D., Tjiputra, J., Walton, J., Wiltshire, A., Winkelmann, R., Wood, R., Yokohata, T., and Ziehn, T.: The TIPMIP Earth system model experiment protocol: phase 1, EGUsphere, 2025, 1–45, https://doi.org/10.5194/egusphere-2025-3604, 2025.

Jones, C. D. and Friedlingstein, P.: Quantifying process-level uncertainty contributions to TCRE and carbon budgets for meeting Paris Agreement climate targets, Environmental Research Letters, 15, 074 019, https://doi.org/10.1088/1748-9326/ab858a, 2020.

https://doi.org/10.5194/egusphere-2026-1673
Preprint. Discussion started: 8 April 2026

Jones, C. D., Arora, V., Friedlingstein, P., Bopp, L., Brovkin, V., Dunne, J., Graven, H., Hoffman, F., Ilyina, T., John, J. G., Jung, M., Kawamiya, M., Koven, C., Pongratz, J., Raddatz, T., Randerson, J. T., and Zaehle, S.: C4MIP – The Coupled Climate–Carbon Cycle Model Intercomparison Project: experimental protocol for CMIP6, Geoscientific Model Development, 9, 2853–2880, https://doi.org/10.5194/gmd-9-2853-2016, 2016.

Jones, C. D., Frölicher, T. L., Koven, C., MacDougall, A. H., Matthews, H. D., Zickfeld, K., Rogelj, J., Tokarska, K. B., Gillett, N. P., Ilyina, T., Meinshausen, M., Mengis, N., Séférian, R., Eby, M., and Burger, F. A.: The Zero Emissions Commitment Model Intercomparison Project (ZECMIP) contribution to C4MIP: quantifying committed climate changes following zero carbon emissions, Geoscientific Model Development, 12, 4375–4385, https://doi.org/10.5194/gmd-12-4375-2019, 2019.

Jones, C. D., Ziehn, T., Anand, J., Bastos, A., Burke, E., Canadell, J. G., Cardoso, M., Ernst, Y., Jain, A. K., Jeong, S., Keller, E. D., Kondo, M., Lauerwald, R., Lin, T.-S., Murray-Tortarolo, G., Nabuurs, G.-J., O'Sullivan, M., Poulter, B., Qin, X., von Randow, C., Sanches, M., Schepaschenko, D., Shvidenko, A., Smallman, T. L., Tian, H., Villalobos, Y., Wang, X., and Yun, J.: RECCAP2 Future Component: Consistency and Potential for Regional Assessment to Constrain Global Projections, AGU Advances, 4, e2023AV001 024, https://doi.org/https://doi.org/10.1029/2023AV001024, 2023.

Kennedy, D., Swenson, S., Oleson, K. W., Lawrence, D. M., Fisher, R., Lola da Costa, A. C., and Gentine, P.: Implementing Plant Hydraulics in the Community Land Model, Version 5, Journal of Advances in Modeling Earth Systems, 11, 485–513, https://doi.org/10.1029/2018MS001500, 2019.

Kim, Y., Moorcroft, P. R., Aleinov, I., Puma, M., and Kiang, N. Y.: Variability of phenology and fluxes of water and carbon with observed and simulated soil moisture in the Ent Terrestrial Biosphere Model (Ent TBM version 1.0.1.0.0), Geoscientific Model Development, 8, 3837–3865, https://doi.org/doi:10.5194/gmdd-8-5809-2015, 2015.

King, J. A., Weber, J., Lawrence, P., Roe, S., Swann, A. L. S., and Val Martin, M.: Global and regional hydrological impacts of global forest expansion, Biogeosciences, 21, 3883–3902, https://doi.org/10.5194/bg-21-3883-2024, 2024.

Koven, C. D., Arora, V. K., Cadule, P., Fisher, R. A., Jones, C. D., Lawrence, D. M., Lewis, J., Lindsay, K., Mathesius, S., Meinshausen, M., Mills, M., Nicholls, Z., Sanderson, B. M., Séférian, R., Swart, N. C., Wieder, W. R., and Zickfeld, K.: Multi-century dynamics of the climate and carbon cycle under both high and net negative emissions scenarios, Earth System Dynamics, 13, 885–909, https://doi.org/10.5194/esd-13-885-2022, 2022.

Kowalczyk, E., Stevens, L., Law, R., Dix, M., Wang, Y., Harman, I., Haynes, K., Srbinovsky, J., Pak, B., and Ziehn, T.: The land surface model component of ACCESS: description and impact on the simulated surface climatology, Australian Meteorological and Oceanographic Journal, 63, 65–82, https://doi.org/10.1071/ES13005, 2013.

Kumarathunge, D. P., Medlyn, B. E., Drake, J. E., Tjoelker, M. G., Aspinwall, M. J., Battaglia, M., Cano, F. J., Carter, K. R., Cavaleri, M. A., Cernusak, L. A., Chambers, J. Q., Crous, K. Y., De Kauwe, M. G., Dillaway, D. N., Dreyer, E., Ellsworth, D. S., Ghannoum, O., Han, Q., Hikosaka, K., Jensen, A. M., Kelly, J. W. G., Kruger, E. L., Mercado, L. M., Onoda, Y., Reich, P. B., Rogers, A., Slot, M., Smith, N. G., Tarvainen, L., Tissue, D. T., Togashi, H. F., Tribuzy, E. S., Uddling, J., Vårhammar, A., Wallin, G., Warren, J. M., and Way, D. A.: Acclimation and adaptation components of the temperature dependence of plant photosynthesis at the global scale, New Phytologist, 222, 768–784, https://doi.org/https://doi.org/10.1111/nph.15668, 2019.

Lasslop, G., Thonicke, K., and Kloster, S.: SPITFIRE within the MPI Earth system model: Model development and evaluation, Journal of Advances in Modeling Earth Systems, 6, 740–755, https://doi.org/https://doi.org/10.1002/2013MS000284, 2014.

Lawrence, D. M., Fisher, R. A., Koven, C. D., Oleson, K. W., Swenson, S. C., Bonan, G., Collier, N., Ghimire, B., van Kampenhout, L., Kennedy, D., Kluzek, E., Lawrence, P. J., Li, F., Li, H., Lombardozzi, D., Riley, W. J., Sacks, W. J., Shi, M., Vertenstein, M., Wieder,

https://doi.org/10.5194/egusphere-2026-1673
Preprint. Discussion started: 8 April 2026

W. R., Xu, C., Ali, A. A., Badger, A. M., Bisht, G., van den Broeke, M., Brunke, M. A., Burns, S. P., Buzan, J., Clark, M., Craig, A., Dahlin, K., Drewniak, B., Fisher, J. B., Flanner, M., Fox, A. M., Gentine, P., Hoffman, F., Keppel-Aleks, G., Knox, R., Kumar, S., Lenaerts, J., Leung, L. R., Lipscomb, W. H., Lu, Y., Pandey, A., Pelletier, J. D., Perket, J., Randerson, J. T., Ricciuto, D. M., Sanderson, B. M., Slater, A., Subin, Z. M., Tang, J., Thomas, R. Q., Val Martin, M., and Zeng, X.: The Community Land Model Version 5: Description of New Features, Benchmarking, and Impact of Forcing Uncertainty, Journal of Advances in Modeling Earth Systems, 11, 4245–4287, https://doi.org/https://doi.org/10.1029/2018MS001583, 2019.

Liddicoat, S. K., Wiltshire, A. J., Jones, C. D., Arora, V. K., Brovkin, V., Cadule, P., Hajima, T., Lawrence, D. M., Pongratz, J., Schwinger, J., Séférian, R., Tjiputra, J. F., and Ziehn, T.: Compatible Fossil Fuel CO2 Emissions in the CMIP6 Earth System Models'Historical and Shared Socioeconomic Pathway Experiments of the Twenty-First Century, Journal of Climate, 34, 2853–2875, https://doi.org/https://doi.org/10.1175/JCLI-D-19-0991.1, 2021.

Lombardozzi, D. L., Bonan, G. B., Smith, N. G., Dukes, J. S., and Fisher, R. A.: Temperature acclimation of photosynthesis and respiration: A key uncertainty in the carbon cycle-climate feedback, Geophysical Research Letters, 42, 8624–8631, 2015.

MacDougall, A. H.: Estimated effect of the permafrost carbon feedback on the zero emissions commitment to climate change, Biogeosciences, 18, 4937–4952, https://doi.org/10.5194/bg-18-4937-2021, 2021.

MacDougall, A. H., Frölicher, T. L., Jones, C. D., Rogelj, J., Matthews, H. D., Zickfeld, K., Arora, V. K., Barrett, N. J., Brovkin, V., Burger, F. A., Eby, M., Eliseev, A. V., Hajima, T., Holden, P. B., Jeltsch-Thömmes, A., Koven, C., Mengis, N., Menviel, L., Michou, M., Mokhov, I. I., Oka, A., Schwinger, J., Séférian, R., Shaffer, G., Sokolov, A., Tachiiri, K., Tjiputra, J., Wiltshire, A., and Ziehn, T.: Is there warming in the pipeline? A multi-model analysis of the Zero Emissions Commitment from CO_2, Biogeosciences, 17, 2987–3016, https://doi.org/10.5194/bg-17-2987-2020, 2020.

Martínez Cano, I., Shevliakova, E., Malyshev, S., Wright, S. J., Detto, M., Pacala, S. W., and Muller-Landau, H. C.: Allometric constraints and competition enable the simulation of size structure and carbon fluxes in a dynamic vegetation model of tropical forests (LM3PPA-TV), Global Change Biology, 26, 4478–4494, https://doi.org/https://doi.org/10.1111/gcb.15188, 2020.

Masson, V., Le Moigne, P., Martin, E., Faroux, S., Alias, A., Alkama, R., Belamari, S., Barbu, A., Boone, A., Bouyssel, F., Brousseau, P., Brun, E., Calvet, J.-C., Carrer, D., Decharme, B., Delire, C., Donier, S., Essaouini, K., Gibelin, A.-L., Giordani, H., Habets, F., Jidane, M., Kerdraon, G., Kourzeneva, E., Lafaysse, M., Lafont, S., Lebeaupin Brossier, C., Lemonsu, A., Mahfouf, J.-F., Marguinaud, P., Mokhtari, M., Morin, S., Pigeon, G., Salgado, R., Seity, Y., Taillefer, F., Tanguy, G., Tulet, P., Vincendon, B., Vionnet, V., and Voldoire, A.: The SURFEXv7.2 land and ocean surface platform for coupled or offline simulation of earth surface variables and fluxes, Geoscientific Model Development, 6, 929–960, https://doi.org/10.5194/gmd-6-929-2013, 2013.

Mathur, S., Agrawal, D., and Jajoo, A.: Photosynthesis: Response to high temperature stress, Journal of Photochemistry and Photobiology B: Biology, 137, 116–126, https://doi.org/https://doi.org/10.1016/j.jphotobiol.2014.01.010, stress and Photosynthesis, 2014.

Matthes, H., Damseaux, A., Westermann, S., Beer, C., Boone, A., Burke, E., Decharme, B., Genet, H., Jafarov, E., Langer, M., Parmentier, F.-J., Porada, P., Gagne-Landmann, A., Huntzinger, D., Rogers, B. M., Schädel, C., Stacke, T., Wells, J., and Wieder, W. R.: Advances in Permafrost Representation: Biophysical Processes in Earth System Models and the Role of Offline Models, Permafrost and Periglacial Processes, 36, 302–318, https://doi.org/https://doi.org/10.1002/ppp.2269, 2025.

Matthews, E.: Global vegetation and land use: new high-resolution data bases for climate studies, Journal of Climate and Applied Meteorology, 22, 474–487, 1983.

Matthews, H. D. and Caldeira, K.: Stabilizing climate requires near-zero emissions, Geophysical Research Letters, 35, https://doi.org/https://doi.org/10.1029/2007GL032388, 2008.

https://doi.org/10.5194/egusphere-2026-1673
Preprint. Discussion started: 8 April 2026

Matthews, H. D., Gillett, N. P., Stott, P. A., and Zickfeld, K.: The proportionality of global warming to cumulative carbon emissions, Nature, 459, 829–832, https://doi.org/10.1038/nature08047, 2009.

Mauritsen, T., Bader, J., Becker, T., Behrens, J., Bittner, M., Brokopf, R., Brovkin, V., Claussen, M., Crueger, T., Esch, M., Fast, I., Fiedler, S., Fläschner, D., Gayler, V., Giorgetta, M., Goll, D. S., Haak, H., Hagemann, S., Hedemann, C., Hohenegger, C., Ilyina, T., Jahns, T., Jimenéz-de-la Cuesta, D., Jungclaus, J., Kleinen, T., Kloster, S., Kracher, D., Kinne, S., Kleberg, D., Lasslop, G., Kornblueh, L., Marotzke, J., Matei, D., Meraner, K., Mikolajewicz, U., Modali, K., Möbis, B., Müller, W. A., Nabel, J. E. M. S., Nam, C. C. W., Notz, D., Nyawira, S.-S., Paulsen, H., Peters, K., Pincus, R., Pohlmann, H., Pongratz, J., Popp, M., Raddatz, T. J., Rast, S., Redler, R., Reick, C. H., Rohrschneider, T., Schemann, V., Schmidt, H., Schnur, R., Schulzweida, U., Six, K. D., Stein, L., Stemmler, I., Stevens, B., von Storch, J.-S., Tian, F., Voigt, A., Vrese, P., Wieners, K.-H., Wilkenskjeld, S., Winkler, A., and Roeckner, E.: Developments in the MPI-M Earth System Model version 1.2 (MPI-ESM1.2) and Its Response to Increasing CO2, Journal of Advances in Modeling Earth Systems, 11, 998–1038, https://doi.org/https://doi.org/10.1029/2018MS001400, 2019.

McDowell, N. G., Sapes, G., Pivovaroff, A., Adams, H. D., Allen, C. D., Anderegg, W. R. L., Arend, M., Breshears, D. D., Brodribb, T., Choat, B., Cochard, H., De Cáceres, M., De Kauwe, M. G., Grossiord, C., Hammond, W. M., Hartmann, H., Hoch, G., Kahmen, A., Klein, T., Mackay, D. S., Mantova, M., Martínez-Vilalta, J., Medlyn, B. E., Mencuccini, M., Nardini, A., Oliveira, R. S., Sala, A., Tissue, D. T., Torres-Ruiz, J., Trowbridge, A. M., Trugman, A. T., Wiley, E., and Xu, C.: Mechanisms of woody-plant mortality under rising drought, CO2 and vapour pressure deficit, Nature Reviews Earth & Environment, 3, 294–308, https://doi.org/10.1038/s43017-022-00272-1, 2022.

McNeall, D., Robertson, E., and Wiltshire, A.: Constraining the carbon cycle in JULES-ES-1.0, Geoscientific Model Development, 17, 1059–1089, https://doi.org/10.5194/gmd-17-1059-2024, 2024.

Meinshausen, M., Meinshausen, N., Hare, W., Raper, S. C. B., Frieler, K., Knutti, R., Frame, D. J., and Allen, M. R.: Greenhouse-gas emission targets for limiting global warming to 2 °C, Nature, 458, 1158–1162, https://doi.org/10.1038/nature08017, 2009.

Mo, L., Zohner, C. M., Reich, P. B., Liang, J., de Miguel, S., Nabuurs, G.-J., Renner, S. S., van den Hoogen, J., Araza, A., Herold, M., Mirzagholi, L., Ma, H., Averill, C., Phillips, O. L., Gamarra, J. G. P., Hordijk, I., Routh, D., Abegg, M., Adou Yao, Y. C., Alberti, G., Almeyda Zambrano, A. M., Alvarado, B. V., Alvarez-Dávila, E., Alvarez-Loayza, P., Alves, L. F., Amaral, I., Ammer, C., Antón-Fernández, C., Araujo-Murakami, A., Arroyo, L., Avitabile, V., Aymard, G. A., Baker, T. R., Bałazy, R., Banki, O., Barroso, J. G., Bastian, M. L., Bastin, J.-F., Birigazzi, L., Birnbaum, P., Bitariho, R., Boeckx, P., Bongers, F., Bouriaud, O., Brancalion, P. H. S., Brandl, S., Brearley, F. Q., Brienen, R., Broadbent, E. N., Bruelheide, H., Bussotti, F., Cazzolla Gatti, R., César, R. G., Cesljar, G., Chazdon, R. L., Chen, H. Y. H., Chisholm, C., Cho, H., Cienciala, E., Clark, C., Clark, D., Colletta, G. D., Coomes, D. A., Cornejo Valverde, F., Corral-Rivas, J., Crim, P. M., Cumming, J. R., Dayanandan, S., de Gasper, A., Decuyper, M., Derroire, G., DeVries, B., Djordjevic, I., Dolezal, J., Dourdain, A., Engone Obiang, N. L., Enquist, B. J., Eyre, T. J., Fandohan, A., Fayle, T. M., Feldpausch, T. R., Ferreira, L. V., Finér, L., Fischer, M., Fletcher, C., Frizzera, L., Gianelle, D., Glick, H. B., Harris, D. J., Hector, A., Hemp, A., Hengeveld, G., Hérault, B., Herbohn, J. L., Hillers, A., Honorio Coronado, E. N., Hui, C., Ibanez, T., Imai, N., Jagodziński, A. M., Jaroszewicz, B., Johannsen, V. K., Joly, C. A., Jucker, T., Jung, I., Karminov, V., Kartawinata, K., Kearsley, E., Kenfack, D., Kennard, D. K., Kepfer-Rojas, S., Keppel, G., Khan, M. L., Killeen, T. J., Kim, H. S., Kitayama, K., Köhl, M., Korjus, H., Kraxner, F., Kucher, D., Laarmann, D., Lang, M., Lu, H., Lukina, N. V., Maitner, B. S., Malhi, Y., Marcon, E., Marimon, B. S., Marimon-Junior, B. H., Marshall, A. R., Martin, E. H., Meave, J. A., Melo-Cruz, O., Mendoza, C., Mendoza-Polo, I., Miscicki, S., Merow, C., Monteagudo Mendoza, A., Moreno, V. S., Mukul, S. A., Mundhenk, P., Nava-Miranda, M. G., Neill, D., Neldner, V. J., Nevenic, R. V., Ngugi, M. R., Niklaus, P. A., Oleksyn, J., Ontikov, P., Ortiz-Malavasi, E., Pan, Y., Paquette, A., Parada-Gutierrez, A., Parfenova, E. I., Park, M., Parren, M., Parthasarathy, N., Peri, P. L., Pfautsch, S., Picard, N., Piedade, M. T. F., Piotto, D., Pitman, N. C. A., Poulsen, A. D., Poulsen, J. R., Pretzsch, H., Ramirez Arevalo, F., Restrepo-Correa, Z.,

https://doi.org/10.5194/egusphere-2026-1673
Preprint. Discussion started: 8 April 2026

Rodeghiero, M., Rolim, S. G., Roopsind, A., Rovero, F., Rutishauser, E., Saikia, P., Salas-Eljatib, C., Saner, P., Schall, P., Schelhaas, M.-J., Schepaschenko, D., Scherer-Lorenzen, M., Schmid, B., Schöngart, J., Searle, E. B., Seben, V., Serra-Diaz, J. M., Sheil, D., Shvidenko, A. Z., Silva-Espejo, J. E., Silveira, M., Singh, J., Sist, P., Slik, F., Sonké, B., Souza, A. F., Stereńczak, K. J., Svenning, J.-C., Svoboda, M., Swanepoel, B., Targhetta, N., Tchebakova, N., ter Steege, H., Thomas, R., Tikhonova, E., Umunay, P. M., Usoltsev, V. A., Valencia, R., Valladares, F., van der Plas, F., Van Do, T., van Nuland, M. E., Vasquez, R. M., Verbeeck, H., Viana, H., Vibrans, A. C., Vieira, S., von Gadow, K., Wang, H.-F., Watson, J. V., Werner, G. D. A., Wiser, S. K., Wittmann, F., Woell, H., Wortel, V., Zagt, R., Zawiła-Niedźwiecki, T., Zhang, C., Zhao, X., Zhou, M., Zhu, Z.-X., Zo-Bi, I. C., Gann, G. D., and Crowther, T. W.: Integrated global assessment of the natural forest carbon potential, Nature, 624, 92–101, https://doi.org/10.1038/s41586-023-06723-z, 2023.

Mulcahy, J. P., Jones, C. G., Rumbold, S. T., Kuhlbrodt, T., Dittus, A. J., Blockley, E. W., Yool, A., Walton, J., Hardacre, C., Andrews, T., Bodas-Salcedo, A., Stringer, M., de Mora, L., Harris, P., Hill, R., Kelley, D., Robertson, E., and Tang, Y.: UKESM1.1: development and evaluation of an updated configuration of the UK Earth System Model, Geoscientific Model Development, 16, 1569–1600, https://doi.org/10.5194/gmd-16-1569-2023, 2023.

Natali, S. M., Holdren, J. P., Rogers, B. M., Treharne, R., Duffy, P. B., Pomerance, R., and MacDonald, E.: Permafrost carbon feedbacks threaten global climate goals, Proceedings of the National Academy of Sciences, 118, e2100163 118, https://doi.org/10.1073/pnas.2100163118, 2021.

Osborne, T., Gornall, J., Hooker, J., Williams, K., Wiltshire, A., Betts, R., and Wheeler, T.: JULES-crop: a parametrisation of crops in the Joint UK Land Environment Simulator, Geoscientific Model Development, 8, 1139–1155, https://doi.org/10.5194/gmd-8-1139-2015, 2015.

Parton, W. J., Stewart, J., and Cole, C.: Dynamics of C, N, P and S in Grassland Soils - A Model, Biogeochemistry, 5, 109–131, 1988.

Phillips, O. L., van der Heijden, G., Lewis, S. L., Lopez-Gonzalez, G., Aragao, L. E. O. C., Lloyd, J., Malhi, Y., Monteagudo, A., Almeida, S., Alvarez Davila, E., Amaral, I., Andelman, S., Andrade, A., Arroyo, L., Aymard, G., Baker, T. R., Blanc, L., Bonal, D., Alves de Oliveira, A. C., Chao, K.-J., Davila Cardozo, N., da Costa, L., Feldpausch, T. R., Fisher, J. B., Fyllas, N. M., Freitas, M. A., Galbraith, D., Gloor, E., Higuchi, N., Honorio, E., Jimenez, E., Keeling, H., Killeen, T. J., Lovett, J. C., Meir, P., Mendoza, C., Morel, A., Nunez Vargas, P., Patino, S., Peh, K. S.-H., Pena Cruz, A., Prieto, A., Quesada, C. A., Ramirez, F., Ramirez, H., Rudas, A., Salamao, R., Schwarz, M., Silva, J., Silveira, M., Slik, J. W. F., Sonke, B., Thomas, A. S., Stropp, J., Taplin, J. R. D., Vasquez, R., and Vilanova, E.: Drought-mortality relationships for tropical forests, New Phytologist, 187, 631–646, https://doi.org/DOI 10.1111/j.1469-8137.2010.03359.x, 2010.

Purves, D. and Pacala, S.: Predictive models of forest dynamics, Science, 320, 1452–1453, 2008.

Rabin, S. S., Magi, B. I., Shevliakova, E., and Pacala, S. W.: Quantifying regional, time-varying effects of cropland and pasture on vegetation fire, Biogeosciences, 12, 6591–6604, https://doi.org/10.5194/bg-12-6591-2015, 2015.

Rabin, S. S., Ward, D. S., Malyshev, S. L., Magi, B. I., Shevliakova, E., and Pacala, S. W.: A fire model with distinct crop, pasture, and non-agricultural burning: use of new data and a model-fitting algorithm for FINAL.1, Geoscientific Model Development, 11, 815–842, https://doi.org/10.5194/gmd-11-815-2018, 2018.

Randerson, J. T., Hoffman, F. M., Thornton, P. E., Mahowald, N. M., Lindsay, K., Lee, Y.-H., Nevison, C. D., Doney, S. C., Bonan, G., Stockli, R., Covey, C., Running, S. W., and Fung, I. Y.: Systematic assessment of terrestrial biogeochemistry in coupled climate-carbon models, Global Change Biology, 15, 2462–2484, https://doi.org/10.1111/j.1365-2486.2009.01912.x, 2009.

Randerson, J. T., Li, Y., Fu, W., Primeau, F., Kim, J. E., Mu, M., Hoffman, F. M., Trugman, A. T., Yang, L., Wu, C., Wang, J. A., Anderegg, W. R. L., Baccini, A., Friedl, M. A., Saatchi, S. S., Denning, A. S., and Goulden, M. L.: The weak land carbon sink hypothesis, Science Advances, 11, eadr5489, https://doi.org/10.1126/sciadv.adr5489, 2025.

https://doi.org/10.5194/egusphere-2026-1673
Preprint. Discussion started: 8 April 2026

Reich, P. B., Sendall, K. M., Stefanski, A., Wei, X., Rich, R. L., and Montgomery, R. A.: Boreal and temperate trees show strong acclimation of respiration to warming, Nature, 531, 633–636, 2016.

Rodriguez-Iturbe, I., Porporato, A., Laio, F., and Ridolfi, L.: Plants in water-controlled ecosystems: active role in hydrologic processes and response to water stress: I. Scope and general outline, Advances in Water Resources, 24, 695–705, https://doi.org/https://doi.org/10.1016/S0309-1708(01)00004-5, 2001.

Romanou, A., Gregg, W. W., Romanski, J., Kelley, M., Bleck, R., Healy, R., Nazarenko, L., Russell, G., Schmidt, G. A., Sun, S., and Tausnev, N.: Natural air-sea flux of CO2 in simulations of the NASA-GISS climate model: Sensitivity to the physical ocean model formulation, Ocean Modelling, 66, 26–44, 2013.

Romanou, A., Romanski, J., and Gregg, W. W.: Natural ocean carbon cycle sensitivity to parameterizations of the recycling in a climate model, Biogeosciences, 11, 1137–1154, 2014.

Romanou, A., Lerner, P., Kiang, N., Aleinov, I., Kelley, M., Miller, R., Russell, G., Ruedy, R., Schmidt, G., Hakuba, M., and Wang, O.: The NASA-GISS ModelE2.1-CC2 ESM: development and simulations, EGUsphere, 2026, 1–113, https://doi.org/10.5194/egusphere-2025-4839, 2026.

Sanderson, B. M., Brovkin, V., Fisher, R. A., Hohn, D., Ilyina, T., Jones, C. D., Koenigk, T., Koven, C., Li, H., Lawrence, D. M., Lawrence, P., Liddicoat, S., MacDougall, A. H., Mengis, N., Nicholls, Z., O'Rourke, E., Romanou, A., Sandstad, M., Schwinger, J., Séférian, R., Sentman, L. T., Simpson, I. R., Smith, C., Steinert, N. J., Swann, A. L. S., Tjiputra, J., and Ziehn, T.: flat10MIP: an emissions-driven experiment to diagnose the climate response to positive, zero and negative CO_2 emissions, Geoscientific Model Development, 18, 5699–5724, https://doi.org/10.5194/gmd-18-5699-2025, 2025.

Schuur, E. A., Abbott, B. W., Commane, R., Ernakovich, J., Euskirchen, E., Hugelius, G., Grosse, G., Jones, M., Koven, C., Leshyk, V., Lawrence, D., Loranty, M. M., Mauritz, M., Olefeldt, D., Natali, S., Rodenhizer, H., Salmon, V., SchÃdel, C., Strauss, J., Treat, C., and Turetsky, M.: Permafrost and Climate Change: Carbon Cycle Feedbacks From the Warming Arctic, Annual Review of Environment and Resources, 47, 343–371, https://doi.org/https://doi.org/10.1146/annurev-environ-012220-011847, 2022.

Schuur, E. A. G., McGuire, A. D., Schädel, C., Grosse, G., Harden, J. W., Hayes, D. J., Hugelius, G., Koven, C. D., Kuhry, P., Lawrence, D. M., Natali, S. M., Olefeldt, D., Romanovsky, V. E., Schaefer, K., Turetsky, M. R., Treat, C. C., and Vonk, J. E.: Climate change and the permafrost carbon feedback, Nature, 520, 171–179, https://doi.org/10.1038/nature14338, 2015.

Séférian, R., Nabat, P., Michou, M., Saint-Martin, D., Voldoire, A., Colin, J., Decharme, B., Delire, C., Berthet, S., Chevallier, M., Sénési, S., Franchisteguy, L., Vial, J., Mallet, M., Joetzjer, E., Geoffroy, O., Guérémy, J.-F., Moine, M.-P., Msadek, R., Ribes, A., Rocher, M., Roehrig, R., Salas-y Mélia, D., Sanchez, E., Terray, L., Valcke, S., Waldman, R., Aumont, O., Bopp, L., Deshayes, J., Éthé, C., and Madec, G.: Evaluation of CNRM Earth System Model, CNRM-ESM2-1: Role of Earth System Processes in Present-Day and Future Climate, Journal of Advances in Modeling Earth Systems, 11, 4182–4227, https://doi.org/https://doi.org/10.1029/2019MS001791, 2019.

Seland, Ø., Bentsen, M., Olivié, D., Toniazzo, T., Gjermundsen, A., Graff, L. S., Debernard, J. B., Gupta, A. K., He, Y.-C., Kirkevåg, A., Schwinger, J., Tjiputra, J., Aas, K. S., Bethke, I., Fan, Y., Griesfeller, J., Grini, A., Guo, C., Ilicak, M., Karset, I. H. H., Landgren, O., Liakka, J., Moseid, K. O., Nummelin, A., Spensberger, C., Tang, H., Zhang, Z., Heinze, C., Iversen, T., and Schulz, M.: Overview of the Norwegian Earth System Model (NorESM2) and key climate response of CMIP6 DECK, historical, and scenario simulations, Geoscientific Model Development, 13, 6165–6200, https://doi.org/10.5194/gmd-13-6165-2020, 2020.

Sellar, A. A., Jones, C. G., Mulcahy, J. P., Tang, Y., Yool, A., Wiltshire, A., O'Connor, F. M., Stringer, M., Hill, R., Palmieri, J., Woodward, S., de Mora, L., Kuhlbrodt, T., Rumbold, S. T., Kelley, D. I., Ellis, R., Johnson, C. E., Walton, J., Abraham, N. L., Andrews, M. B., Andrews, T., Archibald, A. T., Berthou, S., Burke, E., Blockley, E., Carslaw, K., Dalvi, M., Edwards, J., Folberth, G. A., Gedney, N.,

https://doi.org/10.5194/egusphere-2026-1673
Preprint. Discussion started: 8 April 2026

Griffiths, P. T., Harper, A. B., Hendry, M. A., Hewitt, A. J., Johnson, B., Jones, A., Jones, C. D., Keeble, J., Liddicoat, S., Morgenstern, O., Parker, R. J., Predoi, V., Robertson, E., Siahaan, A., Smith, R. S., Swaminathan, R., Woodhouse, M. T., Zeng, G., and Zerroukat, M.: UKESM1: Description and Evaluation of the U.K. Earth System Model, Journal of Advances in Modeling Earth Systems, 11, 4513–4558, https://doi.org/https://doi.org/10.1029/2019MS001739, 2019.

Senf, C., Buras, A., Zang, C. S., Rammig, A., and Seidl, R.: Excess forest mortality is consistently linked to drought across Europe, Nature Communications, 11, 6200, https://doi.org/10.1038/s41467-020-19924-1, 2020.

Shevliakova, E., Malyshev, S., Martinez-Cano, I., Milly, P. C. D., Pacala, S. W., Ginoux, P., Dunne, K. A., Dunne, J. P., Dupuis, C., Findell, K. L., Ghannam, K., Horowitz, L. W., Knutson, T. R., Krasting, J. P., Naik, V., Phillipps, P., Zadeh, N., Yu, Y., Zeng, F., and Zeng, Y.: The Land Component LM4.1 of the GFDL Earth System Model ESM4.1: Model Description and Characteristics of Land Surface Climate and Carbon Cycling in the Historical Simulation, Journal of Advances in Modeling Earth Systems, 16, e2023MS003 922, https://doi.org/https://doi.org/10.1029/2023MS003922, 2024.

Smith, R. S., Mathiot, P., Siahaan, A., Lee, V., Cornford, S. L., Gregory, J. M., Payne, A. J., Jenkins, A., Holland, P. R., Ridley, J. K., and Jones, C. G.: Coupling the U.K. Earth System Model to Dynamic Models of the Greenland and Antarctic Ice Sheets, Journal of Advances in Modeling Earth Systems, 13, e2021MS002 520, https://doi.org/https://doi.org/10.1029/2021MS002520, 2021.

Solomon, S., Plattner, G.-K., Knutti, R., and Friedlingstein, P.: Irreversible climate change due to carbon dioxide emissions, Proceedings of the national academy of sciences, 106, 1704–1709, 2009.

Spitters, C., Toussaint, H., and Goudriaan, J.: Separating the diffuse and direct component of global radiation and its implications for modeling canopy photosynthesis. Part I. Components of incoming radiation, Agricultural and Forest Meteorology, 38, 217–229, https://doi.org/https://doi.org/10.1016/0168-1923(86)90060-2, 1986.

Stock, C. A., Dunne, J. P., Fan, S., Ginoux, P., John, J., Krasting, J. P., Laufkötter, C., Paulot, F., and Zadeh, N.: Ocean Biogeochemistry in GFDL's Earth System Model 4.1 and Its Response to Increasing Atmospheric CO2, Journal of Advances in Modeling Earth Systems, 12, e2019MS002 043, https://doi.org/https://doi.org/10.1029/2019MS002043, 2020.

Sulman, B. N., Phillips, R. P., Oishi, A. C., Shevliakova, E., and Pacala, S. W.: Microbe-driven turnover offsets mineral-mediated storage of soil carbon under elevated CO2, Nature Climate Change, 4, 1099–1102, https://doi.org/10.1038/nclimate2436, 2014.

Sulman, B. N., Shevliakova, E., Brzostek, E. R., Kivlin, S. N., Malyshev, S., Menge, D. N. L., and Zhang, X.: Diverse Mycorrhizal Associations Enhance Terrestrial C Storage in a Global Model, Global Biogeochemical Cycles, 33, 501–523, https://doi.org/https://doi.org/10.1029/2018GB005973, 2019.

Swann, A. L. S., Fung, I. Y., and Chiang, J. C. H.: Mid-latitude afforestation shifts general circulation and tropical precipitation, Proceedings of the National Academy of Sciences, 109, 712–716, https://doi.org/10.1073/pnas.1116706108, 2012.

Takata, K., Emori, S., and Watanabe, T.: Development of the minimal advanced treatments of surface interaction and runoff, Global and Planetary Change, 38, 209–222, https://doi.org/https://doi.org/10.1016/S0921-8181(03)00030-4, 2003.

Valdes, P. J., Armstrong, E., Badger, M. P. S., Bradshaw, C. D., Bragg, F., Crucifix, M., Davies-Barnard, T., Day, J. J., Farnsworth, A., Gordon, C., Hopcroft, P. O., Kennedy, A. T., Lord, N. S., Lunt, D. J., Marzocchi, A., Parry, L. M., Pope, V., Roberts, W. H. G., Stone, E. J., Tourte, G. J. L., and Williams, J. H. T.: The BRIDGE HadCM3 family of climate models: HadCM3@Bristol v1.0, Geoscientific Model Development, 10, 3715–3743, https://doi.org/10.5194/gmd-10-3715-2017, 2017.

Wang, Y. P., Law, R. M., and Pak, B.: A global model of carbon, nitrogen and phosphorus cycles for the terrestrial biosphere, Biogeosciences, 7, 2261–2282, https://doi.org/10.5194/bg-7-2261-2010, 2010.

https://doi.org/10.5194/egusphere-2026-1673
Preprint. Discussion started: 8 April 2026

Ward, D. S., Shevliakova, E., Malyshev, S., and Rabin, S.: Trends and Variability of Global Fire Emissions Due To Historical Anthropogenic Activities, Global Biogeochemical Cycles, 32, 122–142, https://doi.org/https://doi.org/10.1002/2017GB005787, 2018.

Weng, E., Malyshev, S., Lichstein, J., Farrior, C., Dybzinski, R., Zhang, T., Shevliakova, E., and Pacala, S. W.: Scaling from individual trees to forests in an Earth system modeling framework using a mathematically tractable model of height-structured competition, Biogeosciences, 2015.

Wieder, W. R., Bonan, G. B., and Allison, S. D.: Global soil carbon projections are improved by modelling microbial processes, Nature Climate Change, 3, 909 EP –, http://dx.doi.org/10.1038/nclimate1951, 2013.

Wieder, W. R., Lawrence, D. M., Fisher, R. A., Bonan, G. B., Cheng, S. J., Goodale, C. L., Grandy, A. S., Koven, C. D., Lombardozzi, D. L., Oleson, K. W., and Thomas, R. Q.: Beyond Static Benchmarking: Using Experimental Manipulations to Evaluate Land Model Assumptions, Global Biogeochemical Cycles, 33, 1289–1309, https://doi.org/https://doi.org/10.1029/2018GB006141, 2019.

Wiltshire, A. J., Burke, E. J., Chadburn, S. E., Jones, C. D., Cox, P. M., Davies-Barnard, T., Friedlingstein, P., Harper, A. B., Liddicoat, S., Sitch, S., and Zaehle, S.: JULES-CN: a coupled terrestrial carbon–nitrogen scheme (JULES vn5.1), Geoscientific Model Development, 14, 2161–2186, https://doi.org/10.5194/gmd-14-2161-2021, 2021.

Wolf, A., Anderegg, W. R. L., and Pacala, S. W.: Optimal stomatal behavior with competition for water and risk of hydraulic impairment, Proceedings of the National Academy of Sciences, 113, E7222–E7230, https://doi.org/10.1073/pnas.1615144113, 2016.

Xu, C., McDowell, N. G., Fisher, R. A., Wei, L., Sevanto, S., Christoffersen, B. O., Weng, E., and Middleton, R. S.: Increasing impacts of extreme droughts on vegetation productivity under climate change, Nature Climate Change, 9, 948–953, https://doi.org/10.1038/s41558-019-0630-6, 2019.

Xu, L., Saatchi, S. S., Yang, Y., Yu, Y., Pongratz, J., Bloom, A. A., Bowman, K., Worden, J., Liu, J., Yin, Y., Domke, G., McRoberts, R. E., Woodall, C., Nabuurs, G.-J., de Miguel, S., Keller, M., Harris, N., Maxwell, S., and Schimel, D.: Changes in global terrestrial live biomass over the 21st century, Science Advances, 7, eabe9829, https://doi.org/10.1126/sciadv.abe9829, 2021.

Yamori, W., Hikosaka, K., and Way, D. A.: Temperature response of photosynthesis in C3, C4, and CAM plants: temperature acclimation and temperature adaptation, Photosynthesis Research, 119, 101–117, https://doi.org/10.1007/s11120-013-9874-6, 2014.

Yool, A., Popova, E. E., and Anderson, T. R.: MEDUSA-2.0: an intermediate complexity biogeochemical model of the marine carbon cycle for climate change and ocean acidification studies, Geoscientific Model Development, 6, 1767–1811, https://doi.org/10.5194/gmd-6-1767-2013, 2013.

Zarakas, C. M., Swann, A. L. S., Koven, C. D., Smith, M. N., and Taylor, T. C.: Different model assumptions about plant hydraulics and photosynthetic temperature acclimation yield diverging implications for tropical forest gross primary production under warming, Global Change Biology, 30, e17 449, https://doi.org/https://doi.org/10.1111/gcb.17449, 2024.

Zhang, D., Huang, Y., Xiong, J., and Yang, Y.: Vegetation Restoration Potential and Its Hydrological Trade-Offs in Global Drylands Under Historical and Future Climate Scenarios, Earth and Space Science, 12, e2025EA004 564, https://doi.org/https://doi.org/10.1029/2025EA004564, 2025.

Zhang, Q., Ficklin, D. L., Manzoni, S., Wang, L., Way, D., Phillips, R. P., and Novick, K. A.: Response of ecosystem intrinsic water use efficiency and gross primary productivity to rising vapor pressure deficit, Environmental Research Letters, 14, 074 023, 2019.

Zickfeld, K., Eby, M., Matthews, H. D., and Weaver, A. J.: Setting cumulative emissions targets to reduce the risk of dangerous climate change, Proceedings of the National Academy of Sciences, 106, 16 129–16 134, https://doi.org/10.1073/pnas.0805800106, 2009.

https://doi.org/10.5194/egusphere-2026-1673
Preprint. Discussion started: 8 April 2026

Ziehn, T., Chamberlain, M. A., Law, R. M., Lenton, A., Bodman, R. W., Dix, M., Stevens, L., Wang, Y.-P., and Srbinovsky, J.: The Australian Earth System Model: ACCESS-ESM1.5, Journal of Southern Hemisphere Earth Systems Science, 70, 193–214, https://doi.org/10.1071/ES19035, 2020.